Ministry of Higher Education and Scientific Research

University M'Hamed BOUGARA – Boumerdes

Institute of Electrical and Electronic Engineering

Department of Power and Control

Final Year Project Report Presented in Partial Fulfilment of

the Requirements for the Degree of

MASTER

In **Electrical and Electronic Engineering**

Option: **Telecommunication**

Title:

Contribution to the Design of Electromagnetic Power Harvesting System

Presented by:

- **ABED Abdesselem**
- **Menouar BARKAT**

Supervisor:

Pr.AZRAR Arab

ACKNOWLEDGEMENT

First and foremost, we shall thank Allah for providing us the ability and opportunity to fulfill our work experience. We would like to express our sincere gratitude to our supervisor, Pr.AZRAR Arab for his continuous support, patience, motivation, immense knowledge and his extensive understanding in Antennas and Microwave engineering. His guidance helped us in all the time of research and writing of this thesis. We appreciate his commitment and belief in our skills and abilities. Special acknowledge go to our Institute of Electrical and Electronic Engineering in university of M'hamed Bougara, Boumerdes for providing the resources and facilities necessary for the research. We are deeply grateful to our families for their love, patience, and unwavering support. Their encouragement has been a great source of strength throughout this journey. Finally, we would like to thank our friends and colleagues, who have been there to support us, provide feedback, and share in both the highs and lows of this process. Thank you all for your contributions and support.

ABSTRACT

In this report, a compact Rectenna is designed and fabricated with the aim of harvesting RF energy at the frequency of 2.4 GHz. The system consists of a 40mm x 40mm microstrip patch antenna, a Villard voltage doubler for the rectifier circuit designed with HSMS-2850 Schottkey diode for RF application. The rectifier and antenna are joined with a Π-matching network composed of printed lumped components for impedance matching, consisting of a series interdigital capacitor and shunt strip inductors. It should be mentioned that the use of printed lumped components is not found in any literature related to energy harvesting as of the writing of this report. The system has been designed on an FR-4 substrate with thickness of 1.5 mm, a tangent loss of 0.02 and relative permittivity of 4.4. Using an RF generator connected to the energy harvesting circuit, the circuit generates measurable voltage starting from 7dBm input power. The realized circuit gives a DC output voltage of 5.4mV at 20dBm input power with a PCE of $2.916 \times 10^{-6}\%$.

LIST OF FIGURES

LIST OF TABLES

LIST OF ABBREVIATIONS

WiFi: Wireless Fidelity

GSM: Global Systems for Mobile

RADAR: RAdio Detection And Ranging.

RF: Radio Frequency

DC: Direct Current

WPT: Wireless Power Transfer

TV: TeleVision

IoT: Internet of Thing.

RFID: Radio Frequency IDentification.

SHARP: Stationary High Altitude Relay Program

EM: ElectroMagnetic

PCE: Power Conversion Efficiency

ADS: Advanced Design Systems

WPC: Wilkinson Power Combiner

WPD: Wilkinson Power Divider

PIN: Positive-Intrinsic-Negative

ISM: Industrial, Scientific and Medical

PTFE: Polytetrafluoroethylene

CST: Computer Simulation Technology

VNA: Vector Network Analyzer

LIST OF SYMBOLS

Z_{in}: Input Impedance

Z_0: Characteristic impedance of transmission line

P_{DC}: DC power

P_{AC}: AC power

V_{DC}: DC voltage

R_{Load}: Load resistance

Z_L: Load impedance

Ω: Ohm

dB: Decibel

GHz: GigaHertz

pF: Pico Farad

ε_r: Relative permittivity

ε_{re}: Efective Relative Permittivity

nH: nano Henry

CONTENT

GENERAL INTRODUCTION

As the times are advancing, we notice an increased usage of wireless communication media such as radio towers, Wi-Fi (Wireless Fidelity) modems, GSM (Global System for Mobile) and RADARs (Radio Detection and Ranging) resulting in a considerable increase in the amount of ambient RF (Radio Frequency) power density. Moreover, the advancement in electronics have led to invention of small low power devices that would require a small power source to accommodate especially in the medical field for constant health monitoring where using a replaceable battery can be unpractical or even dangerous. Electromagnetic Energy Harvesting System can be a solution for the matter, this system is also called Rectenna which stands for Rectifier-Antenna, it is a system that converts the ambient electromagnetic waves into a usable DC (Direct Current) current that may satisfy these low power needs. This concept was firstly discovered by Nikola Tesla, he was the first to conduct experiment on wireless power transfer, in Colorado Springs, United States, in 1899. This marked the beginning of both WPT (Wireless Power Transfer) and energy harvesting from ambient radio waves technology to start evolving day by day. The receiving antenna is the part of the system that receives the wasted emitted energy from the wireless devices such as s cell-phone towers, laptops, mobile phones, satellite systems, TV (TeleVision) satellites, and Wi-Fi routers. The antenna generates AC (Alternative Current) signal through the collected electromagnetic waves, which will be the input to the rectifier circuit. The rectifier circuit transforms the AC signal to DC signal which will feed a low energy device or it can be used to extend a battery life of other devices. The antenna and the rectifier circuit are connected through a impedance matching network that ensures maximum power transfer. In addition, microstrip technology resulted in a significant size reduction for RF circuitry down to the micrometer scale leading it to be a better choice when compared to other energy harvesting systems (thermal and Piezoelectric).

Chapter 1. State of the Art

1.1 Introduction

Nowadays, harvesting the ambient electromagnetic energy became popular, since it's usable and necessary for powering low-consumption devices (smart watches, sensors, IoT (Internet of Things) devices, RFID (Radio Frequency Identification)), thanks to the rectenna device and the availability of the electromagnetic waves in the environment. In this chapter, we coverer the historical background of the wireless power transfer development, and then we analyze the functionality of each part of the rectenna and the macro level architecture of the system. At the end, the state of the art of the conversion RF-DC circuit and different approaches are mentioned.

1.2 History of wireless energy harvesting

The rectenna was invented by William C. BROWN in the 1950s, it was based on previous researches done by NIKOLA Tesla where he was the first to discover the wireless power transfer of the electromagnetic energy. Figure 1.1 shows WPT (Wireless Power Transfer) drone experiment done by W. C. Brown to restrain a drone in the laboratory in June 1964 [1].

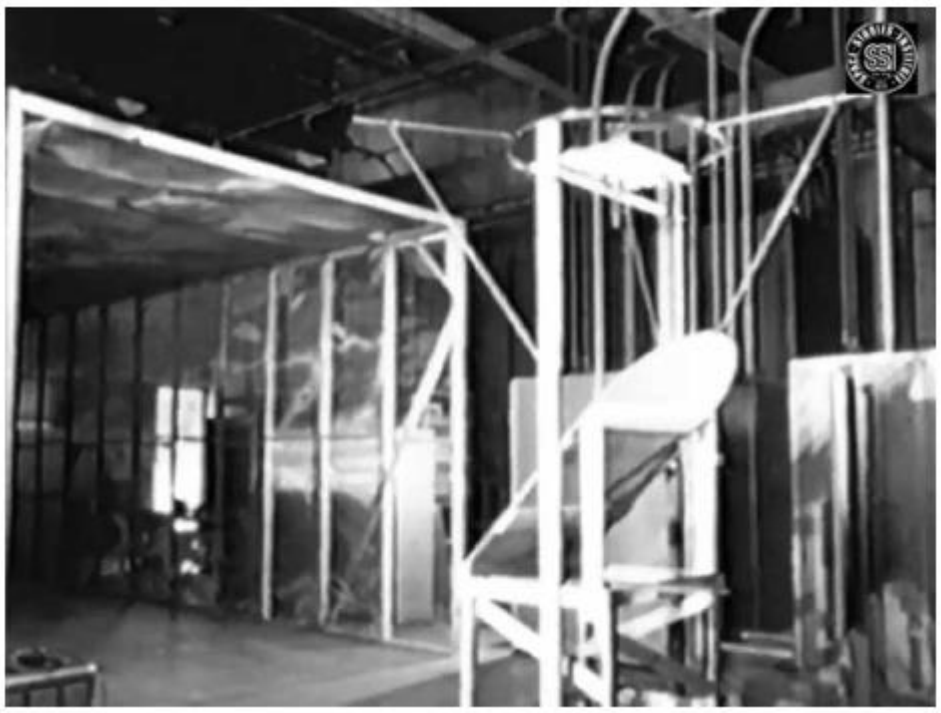

Figure 1.1 Wireless power transfer experiment done by W. C. Brown[1]

Further improvements were made in this filed; Table 1 summarizes the main research development in the history of harvesting electromagnetic energy.

DATE	Researcher's name	Summary	Ref
1862	James Clerk Maxwell	Has proposed a theoretical approach of wireless energy transfer system (WPT).	[2]
1888	Heinrich Hetz	First experimental test demonstrating the possibility of transferring energy between two points.	[3]
1894 1899	Marconi	Demonstrated the possibility of radio transmission over a distance of 2.75 km.	[4]
1894 1899	Tesla	Managed to transmit wirelessly over a distance of around 48 km.	[5]
1901	Tesla	Tesla even designed a tower called Wardenclyffe, 130 km east of New York on Long Island, intended to the Earth's magnetic energy recovery, but which was never tested. The tower was demolished during the First World War.	[6]
1961	Wiliam Brown	Published an article exploring the possibility of microwave power transfer	[7]
1977	Wiliam Brown	Improved the design of rectenna networks by introducing thin-film etched rectennas	[8]
1987	Japan & Canada	A program called SHARP {Stationary High Altitude Relay Program} aimed to realize a prototype airborne platform was carried out in Canada: it flew at an altitude of 150 km for 20 minutes using RF energy at 2.45 GHz with a source placed on the ground. The radiated power density was 400W/m², which provided 150W of power to the electric motor.	[9] [10]
1992	Japan	A model aircraft was piloted using microwave power (MILAX project). Conducted in Japan, this experiment was the first to use a phased array of electronically scanned antennas to direct the microwave beam at 2.411 GHz onto the moving aircraft.	[10]
2000 2002	SPRITZ Program	A WPT system operating at a frequency of 5.77 GHz has been designed to power a network containing 1848 rectennas.	[11]
2000	Texas university A&M	A network of rectennas has been designed, operating at a frequency of 2.8 GHz with a power density of 2 mW/cm² and maximum RF-DC conversion efficiency of 82%.	[12]

Tableau 1.1 History of Electromagnetic wave recovery [13]

1.3 Rectenna architecture

The rectenna is a mean of collecting and converting the energy that is carried by the EM (ElectroMagnetic) waves transmitted by wireless devices such as cell phone tower, phones, Wi-Fi modem. It is composed of the blocks illustrated in Figure 1.2. The antenna collects the RF energy and converts it to an AC signal, while the rectifier circuit converts the AC voltage to DC voltage; both are connected with an impedance matching circuit to ensure maximum transfer of power.

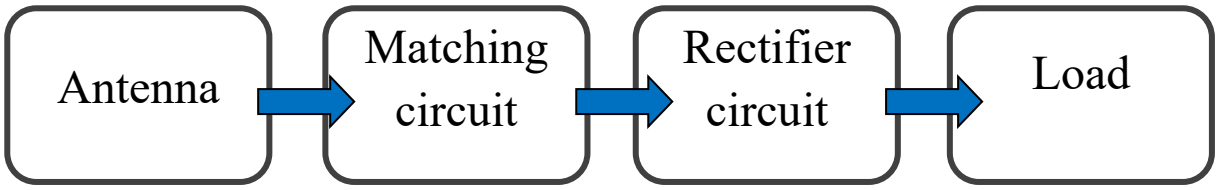

Figure 1.2 Block diagram of a typical power harvesting circuit

The antenna is described in Chapter 2 that contains the design and simulation of the proposed antenna. The rectifier circuit and matching network designs are in Chapter 3.

1.4 Rectifier in literature

In this chapter, different approaches were made in this field by many researchers, whether on the antenna design techniques or the rectifier circuit design. Here, we list few of the previous projects.

1.4.1 Single band rectifier

This research presents a novel high-efficiency rectifier applicable to wireless power transfer and energy harvesting. The proposed rectifier contains several cells; each cell is directly connected to a voltage doubler rectifier, making it possible to directly rectify the microwaves incident on reception (see Figure 1.3). The impedance characteristics and rectification performance of the proposed meta rectification surface are tested using numerical simulation and measurement. The measured results demonstrate an overall PCE (Power Conversion Efficiency) of 76.8% at an incident power of 0.4 dBm [14].

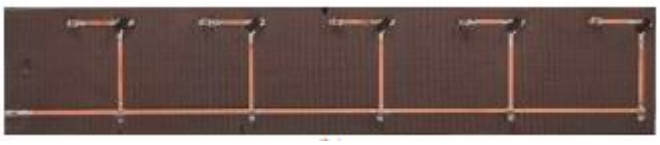

(a) Front view

(b) Back view

Figure 1.3 Fabricated 1 × 5 rectifying Metasurface used in measurement[14]

Figure 1.4 shows the variation of the measured and simulated efficiency as a function of the input power at the frequency of 2.45 GHz and for a load of R_l=300 ohms. The simulation was carried out

using ADS (Advanced Design Systems) software. It can be seen that the simulated efficiency is close to that measured with a slight difference in the incident power level at which maximum efficiency occurs. From the measured data, a maximum efficiency of 76.8% is observed at an incident power level of 0.4 dBm. In addition, an efficiency of at least 40% is maintained for incident power levels of -5 to 4 dBm. The efficiency appears to drop quickly after 0.4 dBm, probably due to impedance mismatch and diode breakdown value at higher power levels.

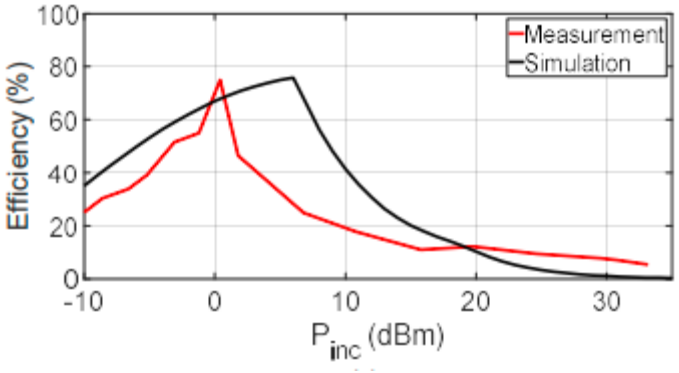

Figure1.4 Plot of the measured efficiency vs input power[14]

1.4.2 Triple-band rectifier

This research presents a novel three-band sensitive power conversion circuit for use in RF energy harvesting systems [15]. The proposed rectifier can simultaneously harvest RF energy from the GSM-900, GSM-1800 and Wi-Fi-2.4 GHz bands at relatively low and medium power levels (see Figure 1.5). The study also presented a new impedance matching technique that improves the efficiency and performance of the rectifier. The proposed rectifier consists of three parallel branches. Each branch includes an input matching circuit designed to provide maximum RF power transferred to the rectifier circuit, a unique voltage doubler using the HSMS-2852 Schottky diodes and a low-pass filter.

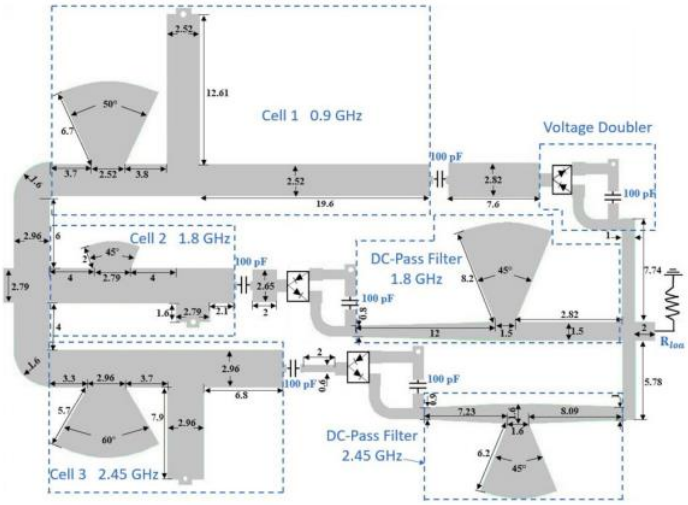

Figure 1.5 Topology of rectifying circuit with a three-branch impedance matching network [15]

A prototype of the proposed rectifier circuit was fabricated-as illustrated in Figure 1.6 and tested to verify its performance against the simulation results. Using an optimal load resistor of 3.8 KΩ with an input power level of -10 dBm, the measured RF to DC conversion efficiency reached 33.7%, 21.8% and 20% at frequencies 0.9GHz, 1.8GHz and 2.45 GHz respectively.

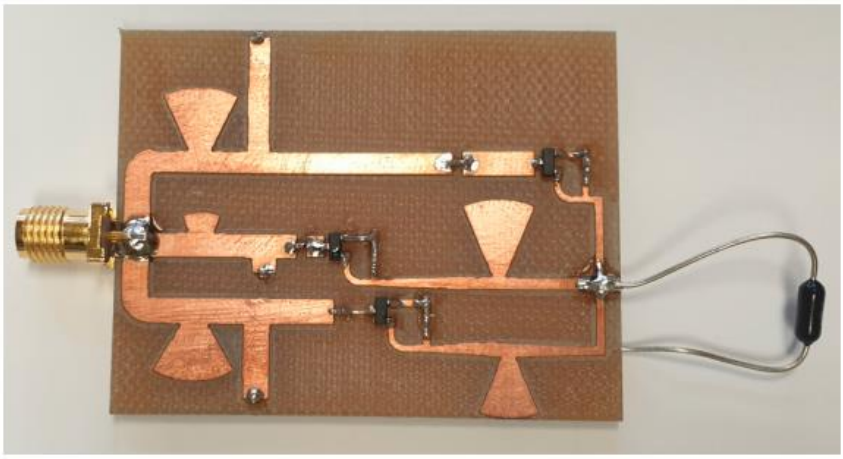

Figure 1.6 Fabricated prototype of the proposed triple-band rectifier [15]

Figure 1.7 shows the measured and simulated reflection coefficients of the triple-band rectifier as a function of frequency at different input power levels from -20 to 0 dBm. Better performance can be achieved at low input power, and the optimal value of reflection coefficient of -17 dB, -22 dB and -31 dB is achieved at 0.9, 1.8 and 2.45 GHz respectively for an input power of -20 dBm. The slight difference between simulated and measured results was mainly due to manufacturing tolerances and measurement connector offset. We can conclude that good impedance matching across all frequencies of interest at different power levels from -20 to 0 dBm is obtained. Figure 1.8 illustrates multiple plots of simulated and measured RF-DC conversion efficiency of the rectifier as a function of RF input power.

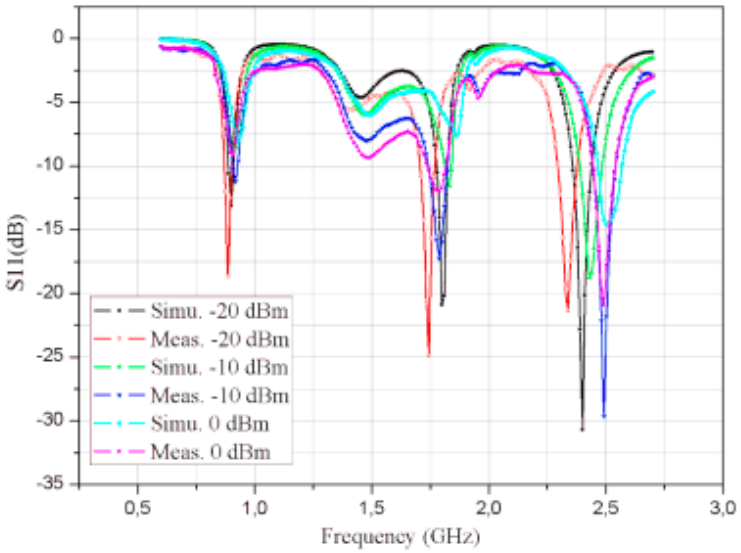

Figure 1.7 Simulated and the measured S11 levels plots of the proposed design[15]

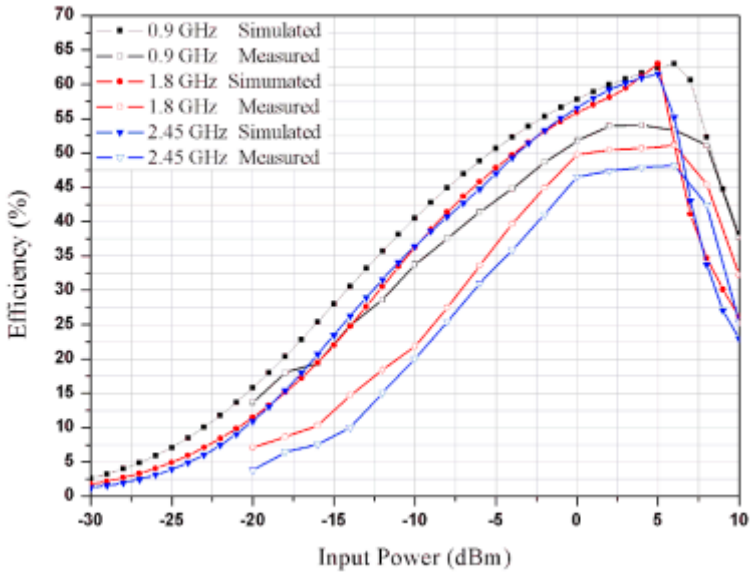

Figure 1.8 The simulated and measured PCE versus RF input power in dBm[15]

1.4.3 Wide-band rectifier

In [16], the designed circuit is made on top of FR-4 substrate material using WPC (Wilkinson Power Combiner) as shown in Figure 1.9. This circuit enables combining two RF signals with different frequency range, and it realized using Chebyshev impedance matching technique on WPD (Wilkinson Power Divider) to achieve broadband operating range, since WPDs are narrow-band structures designed for a single central frequency value.

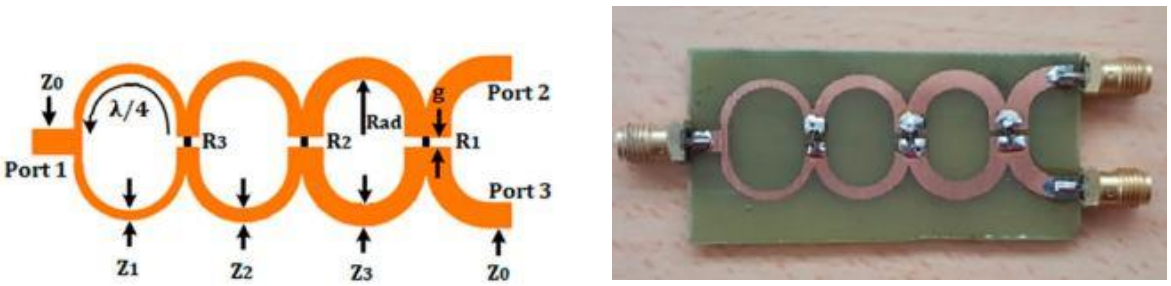

(a) Power divider designed layout **(b)** Fabricated power divider

Figure 1.9 Schematic view of the Chebyshev matched Wilkinson Power Divider [16]

A Greinacher rectifier consisting of Schottky diodes that have good response and low voltage threshold level is used in conjunction with capacitors.

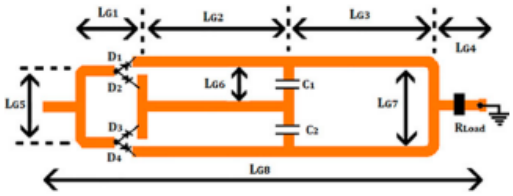

(a) Rectifier circuit designed layout

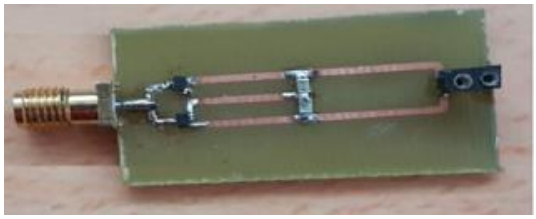

(b) Fabricated rectifier circuit

Figure 1.10 Schematic view of the Greinacher rectifier circuit and the manufactured circuit[16]

In the whole design, the RF rectifier circuit was connected to the WPC circuit in order to direct different RF signals to a single rectifier circuit and reduce the number of circuit elements.

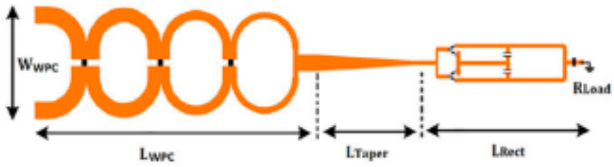

(a) Designed system layout

(b) Fabricated system circuit

Figure 1.11 Schematic view of the WPC-Greinacher design and the manufactured circuit[16]

The results presented in Figures 1.12, 1.13 and 1.14 shows that the design operates on different frequency bands, achieved acceptable efficiency and significant output voltage.

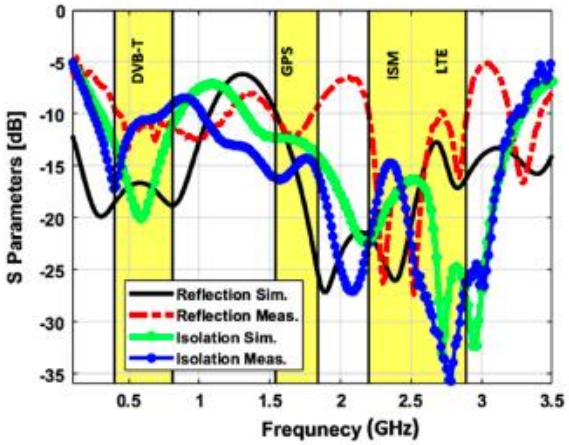

Figure 1.13 Operating frequency of the design[16]

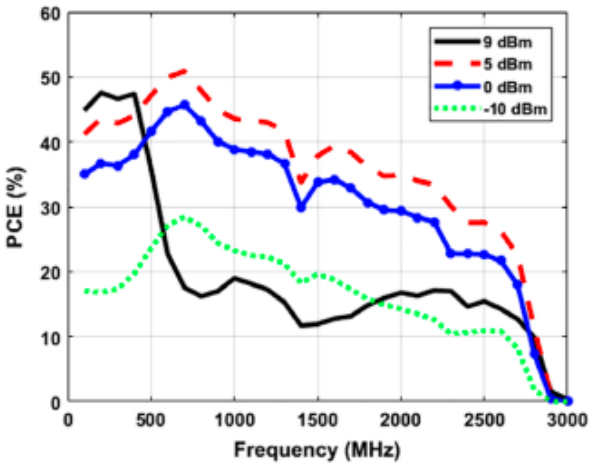

Figure 1.12 Frequency versus PCE graphic of Greinacher rectifier circuit [16]

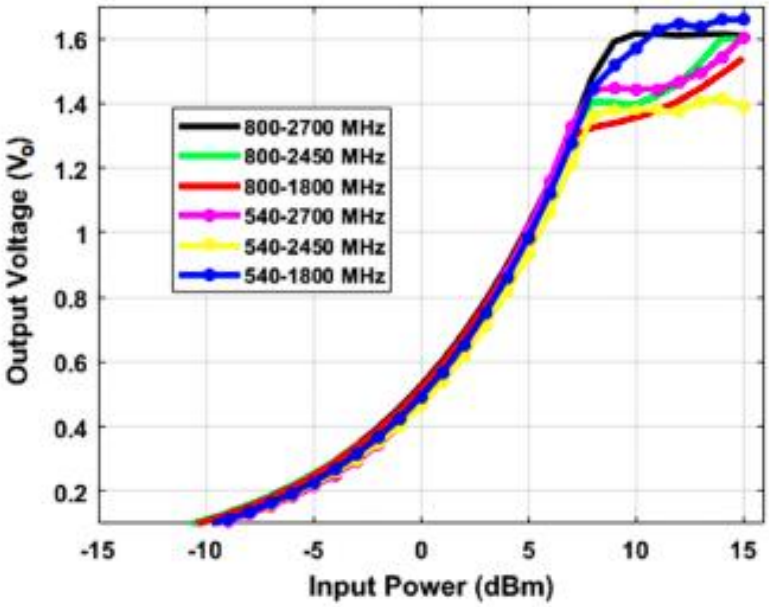

Figure 1.14 Output voltage graph according to different input power values [16]

1.4.4 Variable-band rectifier

Soyeon Jeong presented a rectifier with an intelligent matching circuit based on neural networks for automatic real-time adaptive impedance matching [17]. A matching circuit topology is composed of three consecutive L matching networks consisting of series inductors and shunt capacitors with PIN (positive-intrinsic-negative) diode switches. The simplified diagram of this matching circuit is illustrated in Figure 1.15.

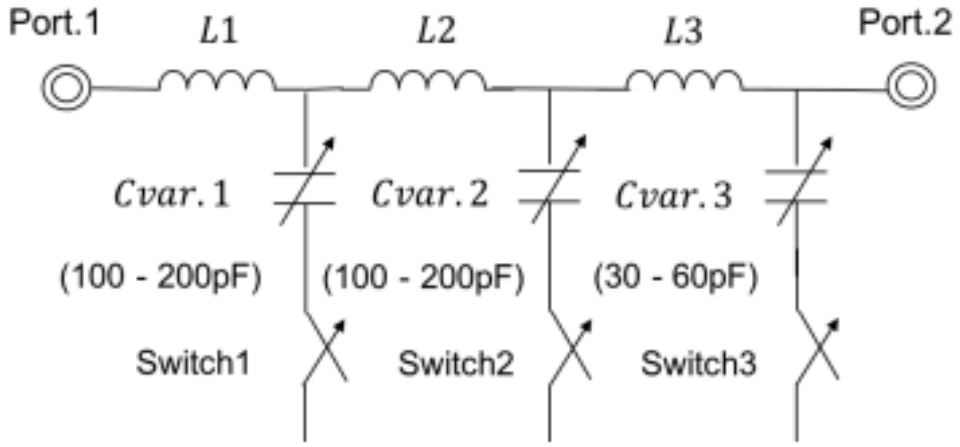

Figure 1.15 Simplified schematic of the automatic matching circuit [17]

Such a technique makes it possible to adapt the rectifier circuit over a wide range of frequencies. Figure 1.16 depicts the variation of |S11| as a function of distance. We notice that the circuit always remains functional despite the variation in the distance between the transmitter and the receiver.

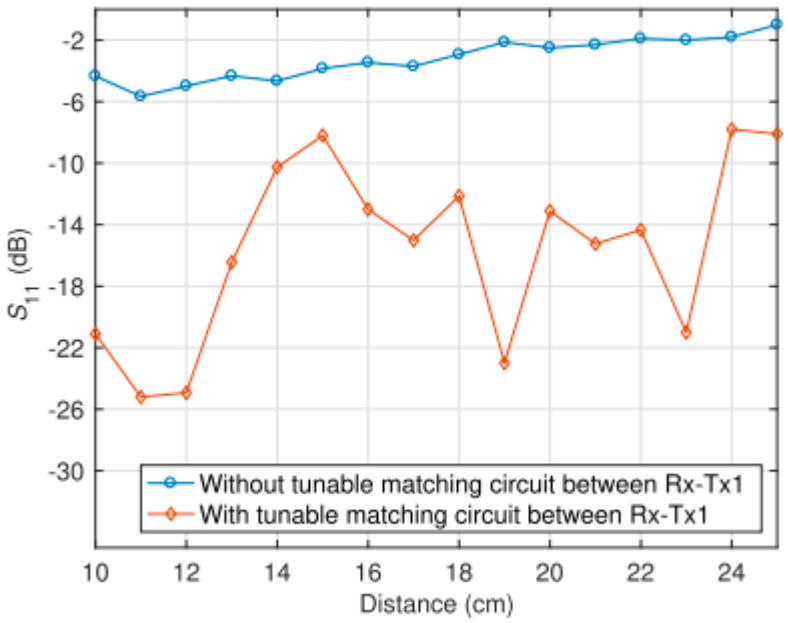

Figure 1.16 Measured values of the reflection coefficient versus frequency[17]

1.4.5 Rectifier implanted on the antenna substrate

A clover shaped rectenna operating in ISM (Industrial, Scientific and Medical) band and exactly at 2.45GHz is presented in [18].The rectifier circuit was implanted on the substrate with the patch antenna as shown in Figure 1.17 which gives the design miniaturized shape and low losses.

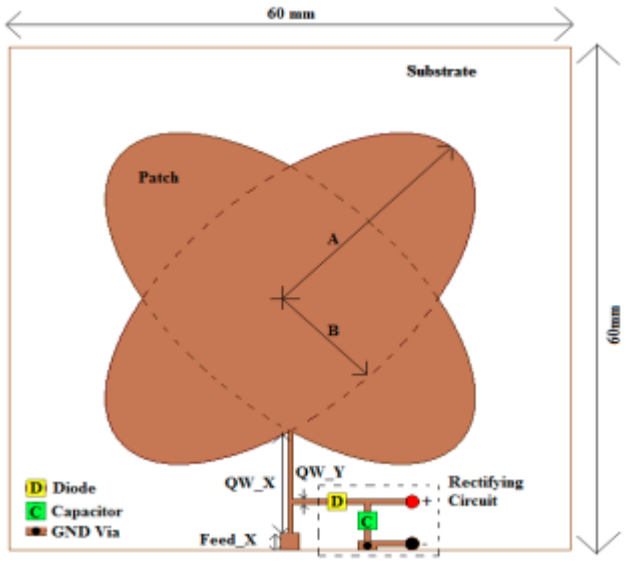

Figure 1.17 Rectenna structure design[18]

A simplified rectifier design was used that consists of Schottky diode that operates in high frequency and a 100nf capacitor that stores and smoothes the DC output waveform.Parametric analysis was done on the patch shape by modeling the antenna dimensions to obtain the desired resonant frequency. The antenna gave narrow bandwidth of 100MHz (2.4-2.5GHZ), with maximum conversion efficiency of 79% and peak gain of 7.19dB as illustrated in Figure1.18.

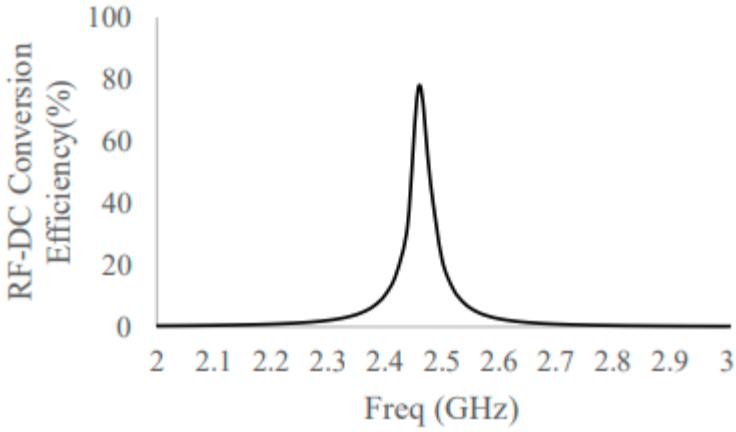

Figure 1.18 RF to DC power conversion efficiency[18]

1.5 Conclusion

At the beginning of this chapter, we introduced the history of electromagnetic energy harvesting and the significant achievements in RF wireless power technologies. Due to technological advancements in recent times, global energy demand has continued to increase and various energy sources remain limited. The use of RF energy harvesting circuits has clearly demonstrated its importance in modern industry and will remain a topic of research for decades to come. Then, we studied the rectenna system, namely the different characteristics of each block constituting this circuit. Finally, we reviewed the different conversion circuits carried out in recent years. Most of these circuits are characterized by high efficiency but only for narrow frequency or power bands, with very low sensitivity.

References

[1] N. Shinohara, J. Zhou, *"Far-Field Wireless Power Transfer and Energy Harvesting",* Artech House Electromagnetic Analysis Library, London, 2023.

[2] J. C. Maxwell, "Dynamical Theory of the Electromagnetic Field", *Philosophical Transactions of the Royal Society of London*, Vol-155, 459-512, in 1865.

[3] H. Hertz, *"dictionary of scientific biography*", New YorkScribner, 1973.

[4] "Marconi Wireless Tel. Co. v. United States, 320 U.S. 1", us supreme court center,1943. [online]. Available: https://supreme.justia.com/cases/federal/us/320/1/.

[5] "Nikola Tesla On His Work with Alternating Currents and Their Application to Wireless Telegraphy, Telephony, And Transmission of Power", Wireless Telegraphy and Telephony. [online]. Available: https://archive.org/details/nikola-tesla-on-his-work-with-alternating-currents-and-their-application-to-wire.

[6] "N. Tesla, The Future of the Wireless Art", Wireless Telegraphy and Telephony. [online]. Available: http://www.tfcbooks.com/tesla/1908-00-00.htm.

[7] W. R. brown, "A survey of the elements of power transmission by microwave beam". *IRE International Convention Record*, Vol. 9, N° 3, p-p 93-105, 1961.

[8] W. C. Brown, "electronic and mechanical improvement of the receiving terminal of a free-space microwave power transmission system", *Raytheon Contractor* Rep. PT-4964, Aug. 1977, NASA CR-135194.

[9] B. Strassner and K. Chang," Microwave Power Transmission: Historical Milestones and System Components", *Proc. IEEE*, vol. 101, No. 6, pp. 1379- 1396, Jun. 2013.

[10] Y. Fujino, T. Ito, N. Kaya, H. Matsumoto, K. Kawabata, H. Sawada, and T. Onodera, 'a rectenna for MILAX', *Proc. Wireless Power Trans*. Conf., pp. 273-277. Feb. 1993.

[11] H. Matsumoto, 'Research on solar power satellites and microwave power transmission in Japan', *IEEE Microw.* Mag, vol. 3, No. 4, pp. 36-45, 2000.

[12] B. Strassner and K. Chang, "5.8 GHz circularly polarized dual rhombic loop traveling wave rectifying antenna for low power density wireless power transmission applications", *IEEE Trans. Microw. Theory Tech. MTT*, vol. 51, No. 5, pp. 1548-1553, May 2003.

[13] A. BENHAMOU, "conception et optimisation d'un circuit de conversion RF-DC multi-bandes pour la récupérationd'énergieEM",Ph. D. dissertation, LINS, USTHB, Alger, 2022.

[14] L. Kanghyeok, S.K. Hong, "RectifyingMeta surface with High Efficiency at Low Power for 2.45GHz Band",*IEEE antennas and wireless propagation letters*,19(12), pp, 2216-2220,

2019.

[15] H. TAFEKIRT, J. PELEGRI-SEBASTIA, A. BOUAJAJ, B. M. REDA,"A Sensitive Triple-Band Rectifier for Energy harvesting application", *IEEE access*, 10.1109/ACCESS.2020.2986797, 2020.

[16] O. Kasar, M. Kahriman, M.A. Gozel, "Application of ultra-wideband RF energy harvesting by using multisession Wilkinson power combiner". *Int J RF Microw Compute Aided Eng*, 2018.

[17] S. Jeong, T.H. Lin, M.M.Tentzeris, "A Real-Time Range-Adaptive Impedance Matching Utilizing a Machine Learning Strategy Based on Neural Networks for Wireless Power transfer system", *IEEE Transactions on Microwave Theory and Techniques*, VOL. 67, NO. 12, 2019.

[18] N.R. Kumar, P.D. Sathya, “Design of RF Energy Harvesting Patch Antenna for wireless communications”, *International Journal of Innovative Technology and Exploring Engineering (IJITEE*), Vol-8 Issue-10, August 2019.

Chapter 2. Antenna Design

2.1 Introduction

The antenna is a key element in the RF energy harvesting system. It acts as a transducer, transforming electrical energy into electromagnetic waves and vice versa. Many types of antennas exist, such as wire antennas, aperture antennas, reflectors, and arrays. However, the microstrip antenna is the most recommended and commonly used due to its compact size, flexibility, durability, and low manufacturing cost[1].

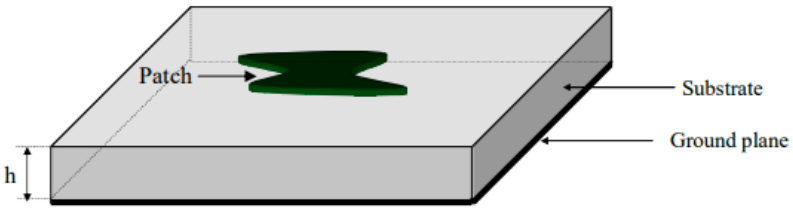

Figure 2.1 Microstrip antenna structure [2]

To select the best antenna for this field, it is necessary to focus on the following parameters.

2.2 Directivity and Gain

The directivity represents the ability of the antenna to focus the transmission (or the reception) in a specific direction; it is essentially the ratio between the radiation intensity in a specific direction and the average intensity across all directions[2]. The higher the directivity, the narrower is the beamwidth, the more directional the antenna is. An antenna is said to be isotropic if it receives the signal in all direction with the same amount.

As for the gain, it is an important parameter that describes the performance of the antenna in sending and receiving power; it is defined as the ratio of the radiation intensity in a given direction, to the total input (accepted) power. The gain signifies the amount of the power that can be transmitted compared to the received (input).

2.3 Reflection Coefficient

The reflection coefficient, symbolized by Γ (or S11 as S-parameter), it is the measure that describes the reflecting of signal happening at the input of the antenna due to the impedance mismatch between the transmission line and the antenna[2]. It can be defined by the following formula:

$$\Gamma = \frac{Z_{in} - Z_0}{Z_{in} + Z_0} \tag{2.1}$$

With $Z_0 = 50\Omega$ being the feed line characteristic impedance.

2.4 Radiation pattern

The antenna radiation pattern is the graphical representation (or mathematical function) of the antenna radiation properties in the far field, such as power flux density, radiation intensity, field strength, directivity, phase or polarization as a function of spatial coordinates, i.e. the way the antenna transmits or receives its signal. It is usually represented in logarithmic scale (dB) since it emphasizes the small details of the pattern more than the linear scale.

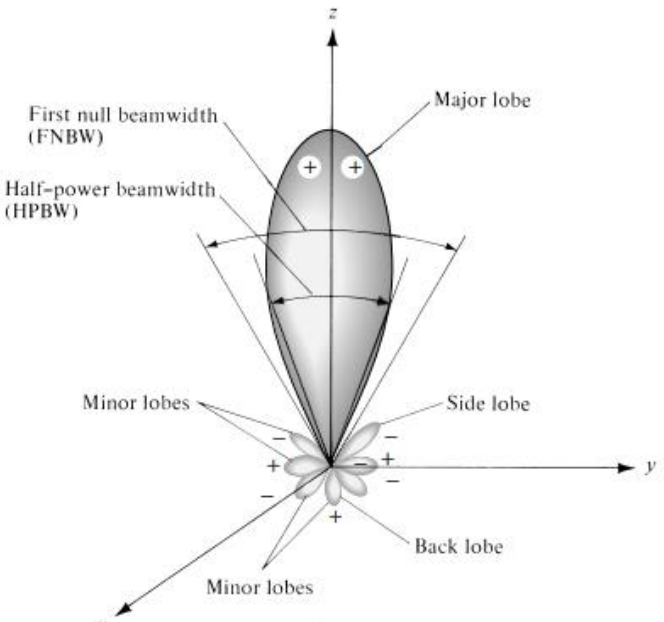

Figure 2.2 Radiation lobes and beamwidths of an antenna radiation pattern [3]

2.5 Input Impedance

The input impedance is defined as the impedance seen by the excitation circuit at the antenna terminals. It is important at the matching level to insure maximum power transfer. The ratio of the voltage to the current at terminals a-b defines the input impedance[2]:

$$Z_{in} = R + jX \tag{2.2}$$

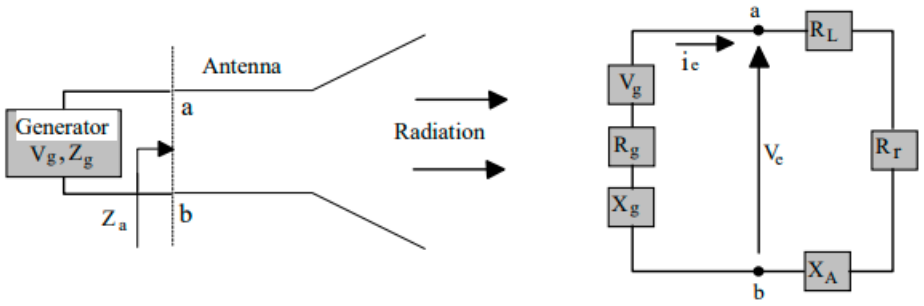

Figure 2.3 Antenna equivalent electrical circuit [2]

The input impedance varies by varying the feeding point, in [3] it was shown that the closer the feeding point is to the center of the patch, the smaller the input impedance becomes, and vice versa. That what will help later to obtain the desired input impedance.

2.6 Antenna Bandwidth and Resonant Frequency

The antenna bandwidth is defined as the range of frequency in which the antenna can perform, which is the range where the magnitude of the reflection coefficient value lay below -10dB, it can be evaluated with the following formula:

$$BW\% = 200\frac{f_2 - f_1}{f_2 + f_1} \tag{2.3}$$

Where f_1 and f_2 are the lower and the higher frequencies respectively at which the value of $|S_{11}| = -10\ dB$. The resonant frequency is the value of frequency that has the lowest value of $|S_{11}|$.The frequency is inversely proportional to the antenna size[2], this will help later in fixing the desired resonant frequency for our antenna.

2.7 Feeding Techniques

There are at least four methods for feeding an antenna[4]. The feeding method is a mean to connect the antenna with either a transmitter or receiver. The most common methods are: microstrip line, coaxial probe, aperture coupling and proximity coupling.

2.7.1 Coaxial feed technique

Because the coaxial feed technique is used in this study, it is detailed in this section. In the coaxial-line feed the inner conductor of the coaxial line is attached to the radiation patch while the outer conductor is connected to the ground plane as shown in Figure 2.4. It is widely used in practice since it is easy to fabricate and match and it has low spurious radiation. However, it has narrow bandwidth and it is more difficult to model, especially for thick substrates (h > 0.02λ0)[3].

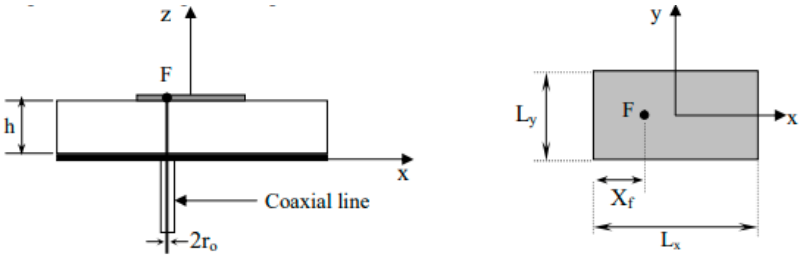

Figure 2.4 Coaxial probe feeding method [2]

2.8 Antenna design procedure

The designed patch looks like clover leaf inspired from reference [5]. It has been designed by properly inserting two identical ellipses with their major axes lie along *x*- and *y*-directions and centered at the origin. The substrate material used is FR4 that has relative permittivity of 4.3 and loss tangent of 0.025, with dimensions of 40 mm for width and length. The antenna is linearly polarized and excited with a coaxial feeding positioned along the *x*-axis as illustrated in Figure 2.5.The coaxial probe feed has a pin radius of $R_{pin} = 0.55mm$,and outer coat with radius of $R_{COAT} = 1.95mm$. The space between the pin and the coat is filed with PTFE (Polytetrafluoroethylene), which is a dielectric materiel that has relative of permittivity of 2.1. The length of the major axis is the essential parameter that controls the resonant frequency. The design on the simulating software is made in such a manner the minor axis is varying in accordance with

major axis. At any resonant frequency, the minor axis length is half that of the major axis. Matching the patch to a 50Ω coaxial feed line is done by proper choice of the feed point position along the *x*-axis.

To obtain the required resonant frequency, parametric study on the patch dimension and feed point is carried out and the best obtained values are: major axis length is 37.50 mm and the feed point position at $X_p = 5.50$ mm.

.

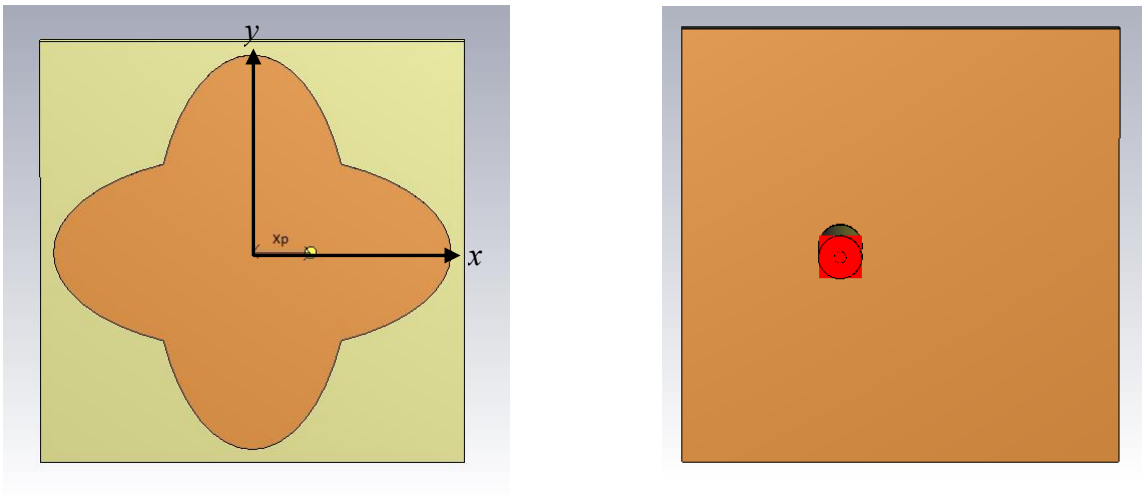

Figure 2.5 Top and back view of the proposed microstrip antenna

The simulation of the obtained antenna is done using CST (Computer Simulation Technology) software, in terms of the input reflection coefficient is shown in Figure 2.6. The figure shows clearly that the designed antenna resonates at the required frequency, exactly at 2.401GHz, with satisfactory reflection coefficient (-31.66dB) indicating good choice of the feed point position. The simulated antenna bandwidth is 57.62 MHz or 2.4%.

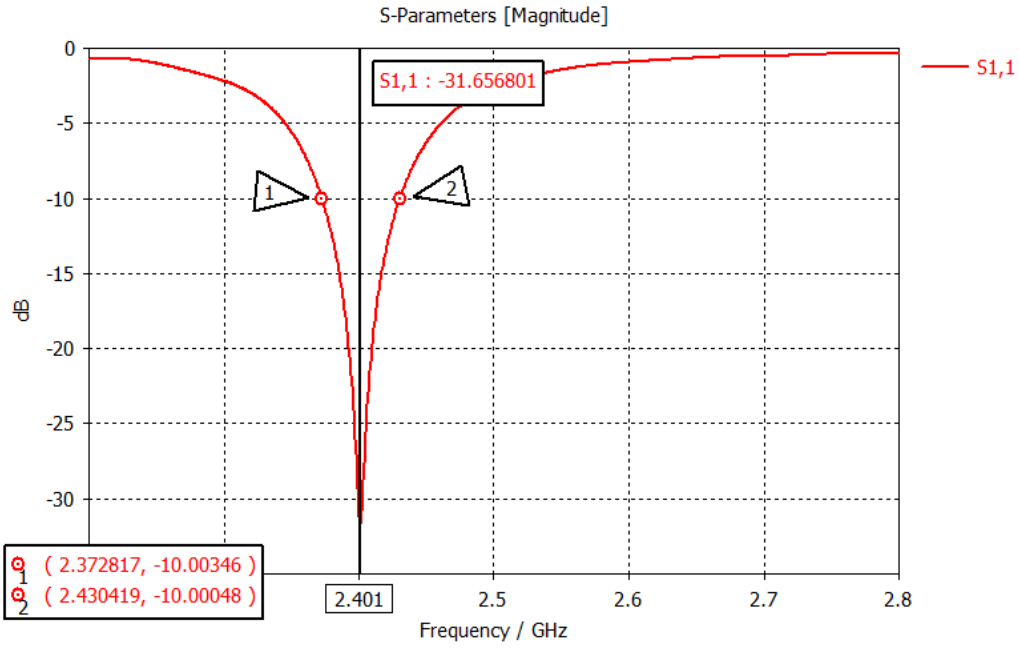

Figure 2.6 Input reflection coefficient of the simulated design versus frequency

Since the input impedance is needed in the design of the matching circuit design, its value versus frequency is illustrated in Figure 2.7. At 2.4GHz frequency the matching network has to match the rectifier impedance to the antenna input impedance of $50.03 + j2.61\ \Omega$.

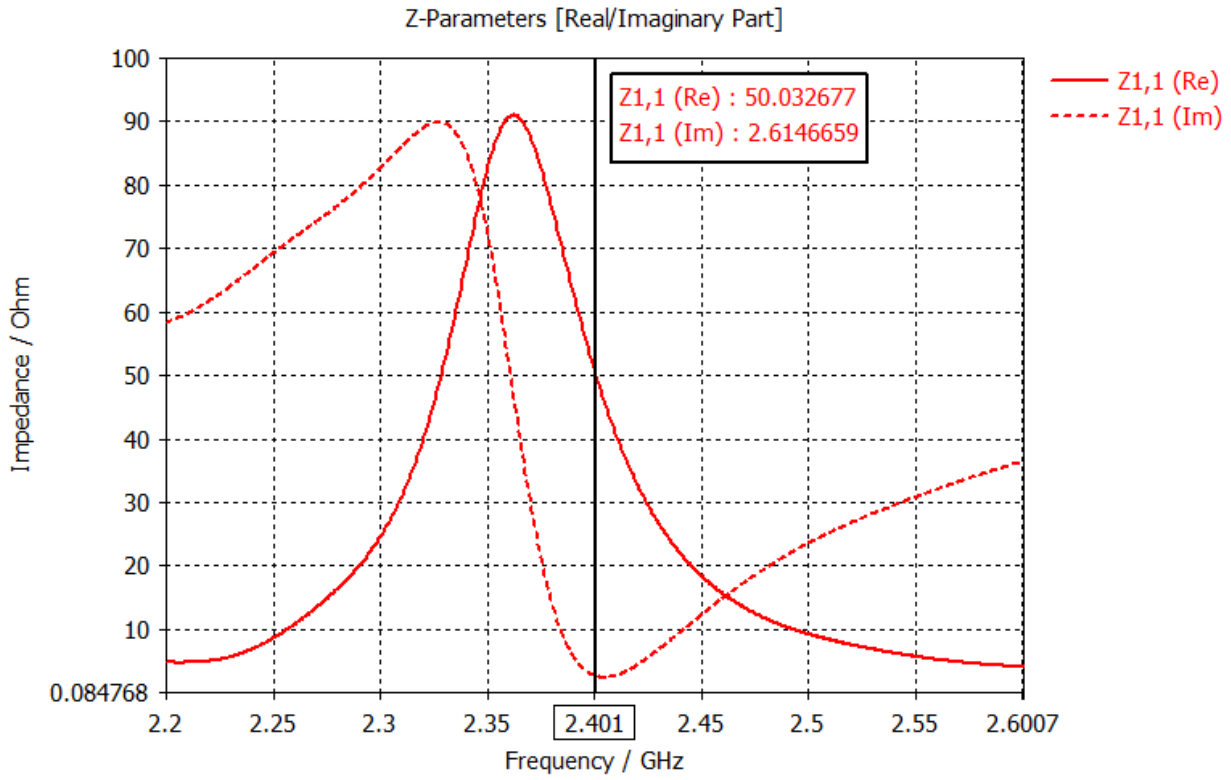

Figure 2.7 Real and imaginary parts of the input impedance versus frequency of the antenna

The current distribution of the antenna at 2.40 GHz is shown in Figure 2.8. It is apparent from the figure that the current is null at the 4 outer corners of patch and maximum at the inner corners. The distance between two successive outer corners seems to be the resonating lengths. The middle of the patch has very low current density since the patch shape is closer to circular than rectangular. We should remember that as the shape is circular the modes are controlled by the roots of either the first kind Bessel functions or their derivatives.

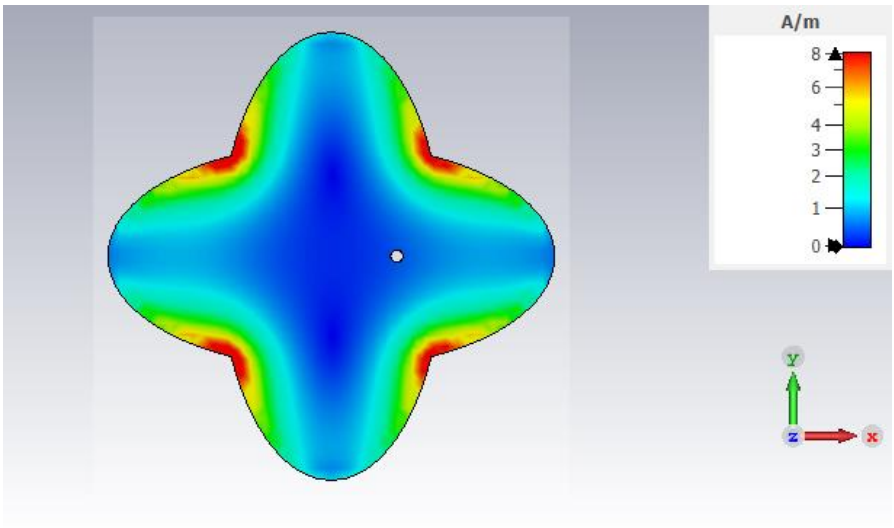

Figure 2.8 Surface current distribution of the antenna structure

The 3D radiated electric far field of the antenna is illustrated in Figure 2.9. This result shows that the antenna is unidirectional with little back lobe resulting from the finite ground plane.

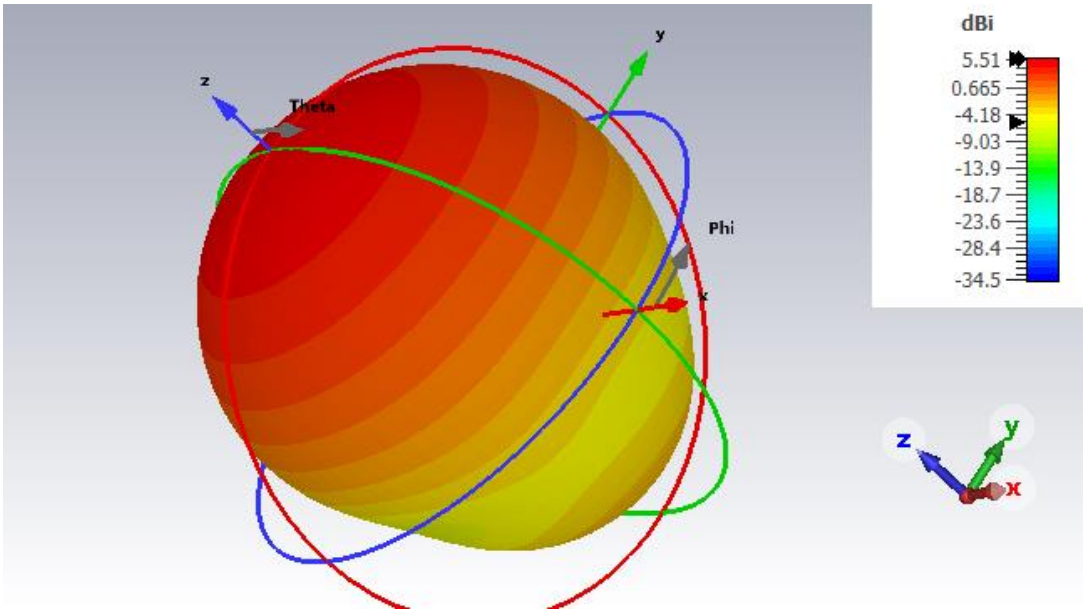

Figure 2.9 3D radiation pattern of the antenna

For having better detail of the radiation characteristics of the antenna, cuts of the 3D pattern in the E- ($\phi = 0$) and H-($\phi = \pi/2$) plans is carried out to obtain the 2D patterns illustrated in Figure 2.10. The remarks given in the 3D pattern are confirmed in the 2D patterns. Also, the figure indicates clearly that the antenna is working at the lowest (fundamental) mode since the upper hemisphere pattern has unique and uniform lobe.

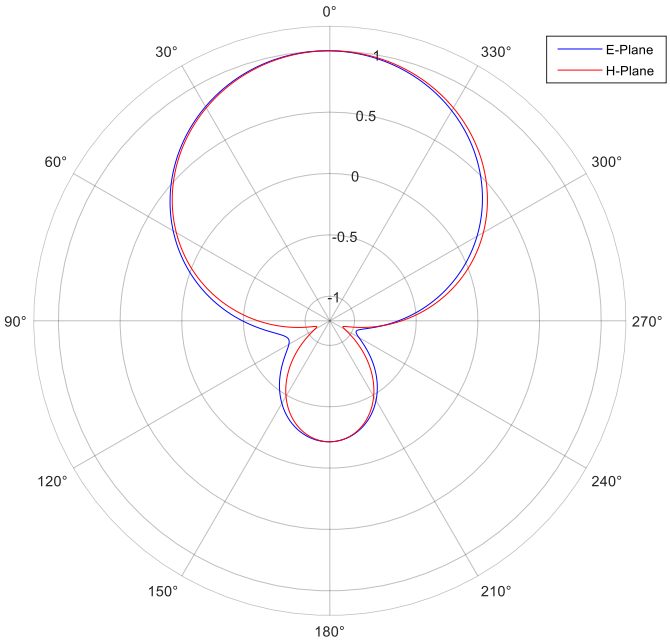

Figure 2.10 E and H plane field patterns of the proposed antenna

To have idea about the polarization purity[3], both the co-polar and cross-polar components of the electric field are drawn in figures 2.11 and 2.12. The E-plane components are illustrated in figure 2.11; in which we see clearly the cross polar component is very low as compared to the co-polar component. Also, the H-plane components illustrated in figure 2.12 shows that the cross polar component is very low compared to the co-polar component.

The quantitative description of the radiation properties of the proposed antenna is summarized in Table 2.1.

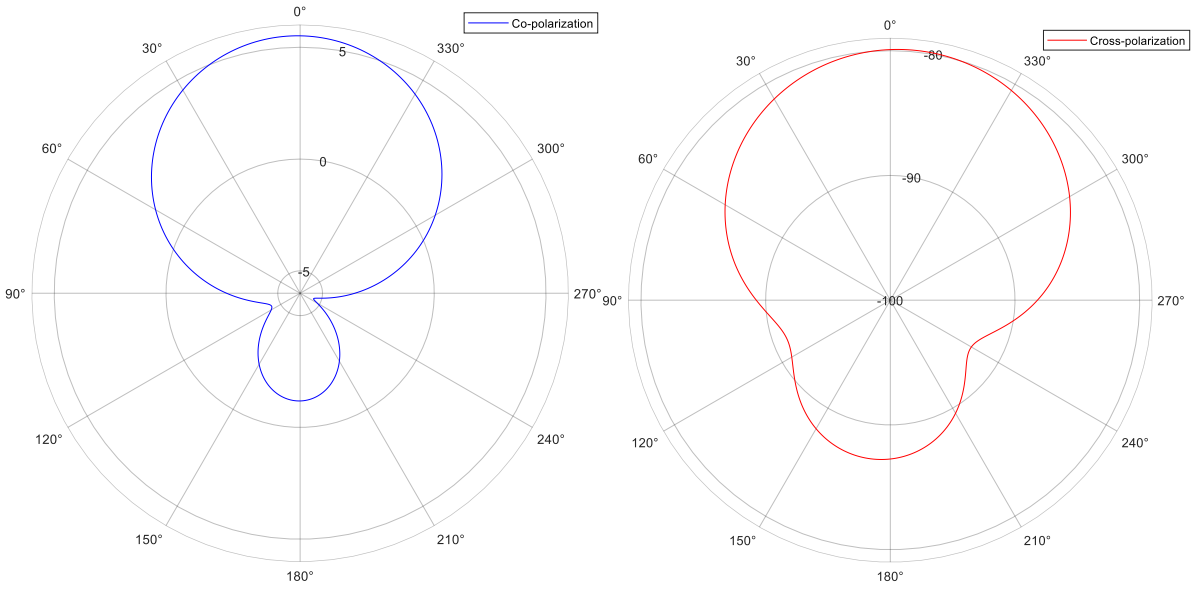

Figure 2.11 Co and Cross polarization components of the electric filed in the E-plane

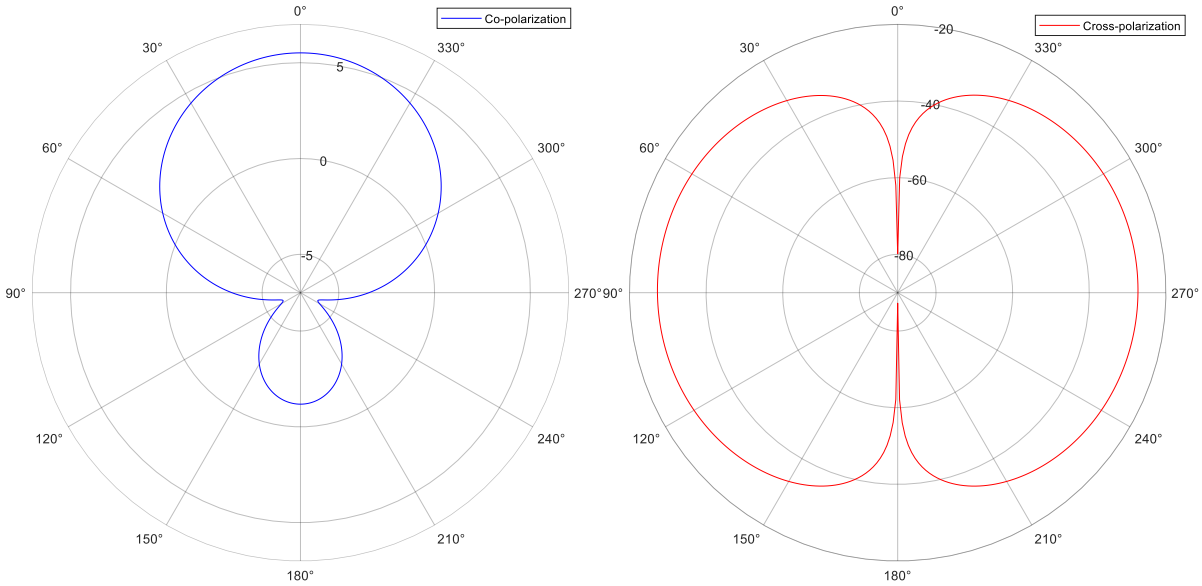

Figure 2.12 Co and Cross polarization components of the electric field in the H-plane

plane	Max co-polar component (dBi)	Max cross-polar component (dBi)	HPBW	Max directivity (dBi)	Max realized gain (dBi)
E (ϕ =0°)	5.25 at θ=1°	-79.9 at θ= -6°	101.0°	5.52 at θ =1°	0.768 at θ=1°
H(ϕ =90°)	5.51 at θ=0°	-27.3 at θ= -85°	99.4°	5.51 at θ = 0°	0.766 at θ = 0°

Table 2.1 Quantitative description of the radiation properties of the antenna

2.9 Conclusion

This chapter details the design of our microstrip patch antenna for 2.4 GHz operation. The designed antenna utilizes FR-4 substrate and a coaxial probe feed for efficient power delivery. Simulations confirm successful performance, achieving both narrow bandwidth with low reflections and good impedance matching, as desired for Electromagnetic harvesting applications in the 2.4 GHz ISM band.

REFERENCES

[1] B.K.Kanaujia, N. Singh, and S. Kumar, "*Rectenna: Wireless Energy Harvesting System*", y Springer Nature Singapore Pte Ltd, 2021.

[2] A. AZRAR, "Antenna Course", Institute of Electrical and Electronic Engineering, University M'hamed BOUGARA, Boumerdes, 2023.

[3] C.A. Balanis, "*Antenna Theory: Analysis and Design*", John Willy & Sons,4th ed. 2016.

[4] C. TAOUINT, "Contribution to The Design and Analysis of Butterfly Printed Antenna," M.S. thesis, Institute of Electrical and Electronic Engineering, University M'Hamed BOUGARA Boumerdes, 2022.

[5] N.R. Kumar, P.D. Sathya, "Design of RF Energy Harvesting Patch Antenna for wireless communications", *International Journal of Innovative Technology and Exploring Engineering (IJITEE)*, Vol-8 Issue-10, August 2019.

Chapter 3. Energy Harvesting Circuit Design

3.1 Introduction

The energy harvesting circuit consists of a rectifier for AC to DC conversion and boosting, and a matching network to match the impedance of the antenna and ensure maximum power transfer while having low losses. A Π matching network with shunt inductors and a series capacitor has been chosen to provide control over the bandwidth of the circuit and block DC from flowing back to the RF source. A new approach that was never done before in an energy harvesting system consists of using interdigital components instead of regular lumped components.

3.2 Rectifier Circuit

A rectifier is a nonlinear circuit that converts an AC signal into a DC signal using a configuration of capacitors and switches which consist of either transistors or diodes. The rectifier uses switches to modify the AC signal in order to generate a DC component like applying the absolute value function using a full bridge rectifier or removing the positive or the negative side of the signal with a half bridge rectifier, then the capacitors work as envelope detectors that ideally will be charged to a constant value that corresponds to the amplitude of the signal.

3.2.1 Rectifier Basics

A basic rectifier circuit and the different waveforms at each stage are shown in Figure 3.1 and 3.2 respectively.

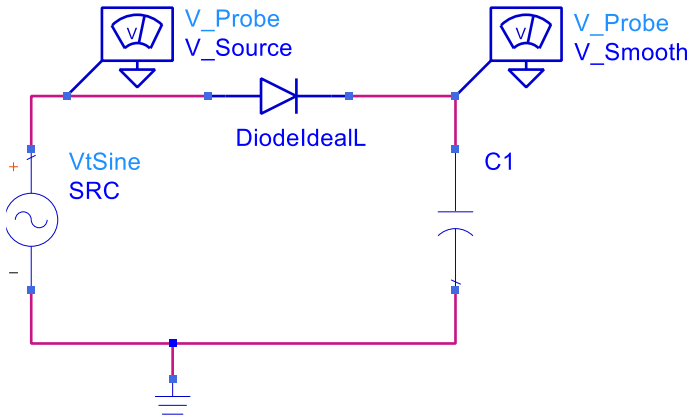

Figure 3.1 Basic rectifier circuit schematic

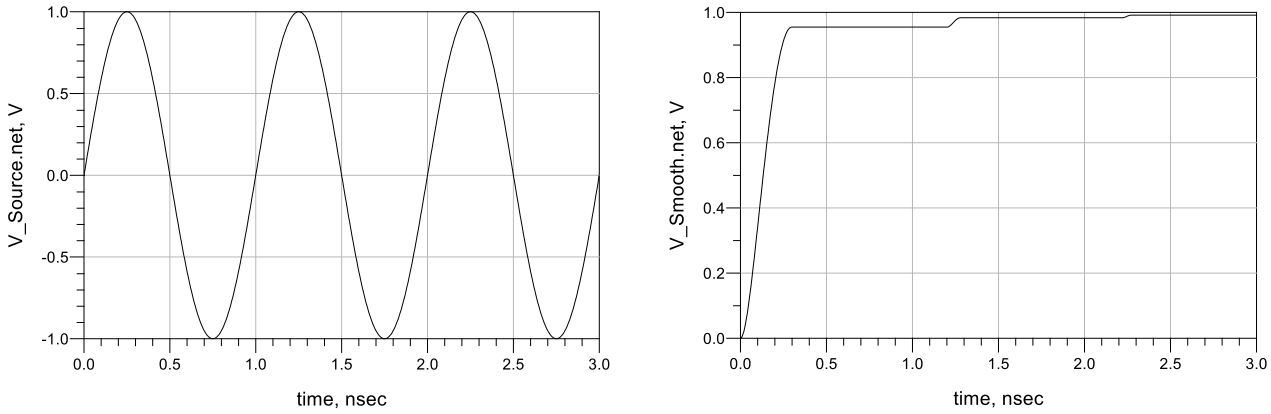

Figure 3.2 Source signal (Left) and rectified signal (Right) waveforms

As shown in Figure 3.2, the capacitor voltage (V_Smooth) is stable at a constant level due to the absence of a load resistor (R=∞) across the capacitor which creates a large time constant $\tau = RC$ causing the capacitor to never discharge. Taking a more practical approach, the presence of parasitic resistances in the capacitor package in addition to load resistance will result in a finite value for the time constant and discharging will occur causing the maximum DC voltage to decrease and ripples to be generated. Figure 3.3 depicts the effect of introducing a resistive load on the rectified signal.

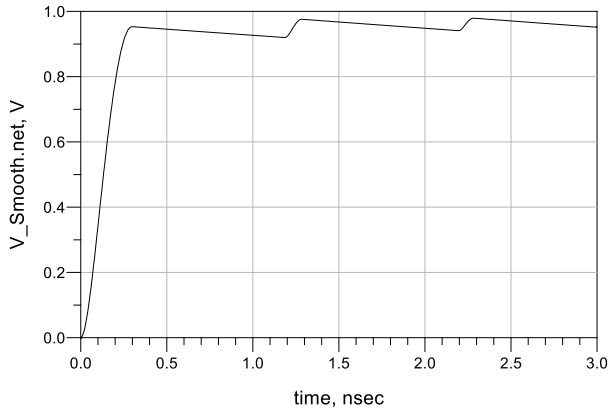

Figure 3.3 Effect of load resistor on the rectified

The effect of discharging can be reduced using a larger capacitor and resistor which increases the time constant τ. Inspecting the frequency spectrum of the rectified signal will give us better understanding of the effect the rectifier has on the frequency of the signal and what frequencies might be generated due to nonlinearity of the rectifier. The frequency spectrums of source signal and rectified signal are shown in Figure 3.4.

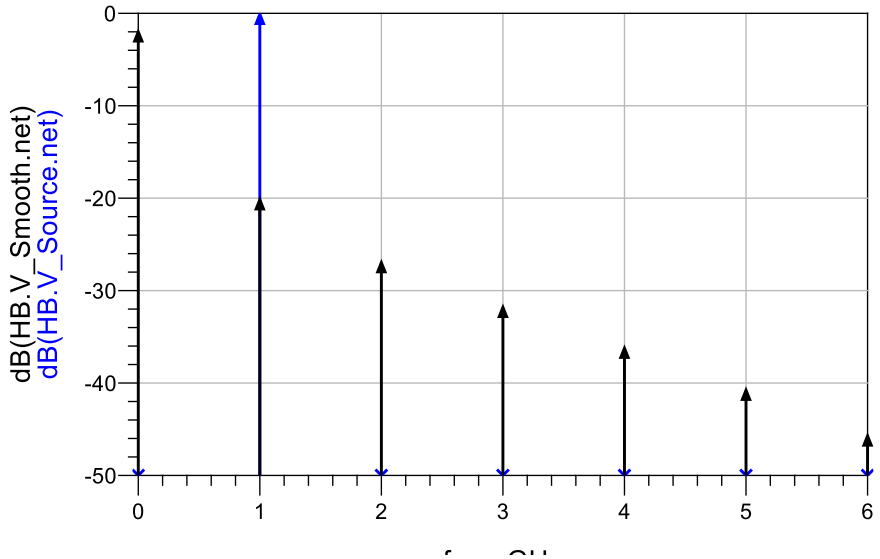

Figure 3.4 Frequency Spectrum of source and rectified signal in dB

As Figure 3.4 depicts, it is noticeable that most of the amplitude of the source signal was shifted to the origin of the frequency spectrum i.e. the DC component of the rectified signal while also introducing harmonics that reduce the magnitude of the DC component and causes ripples in the rectified signal. A rectifier is characterized by its ability to convert AC power into DC power which is known as PCE and defined as the ratio of output DC power to the input AC power.

$$\mathrm{PCE}(\%) = \frac{\mathrm{P_{DC}}}{\mathrm{P_{AC}}} = \frac{{\mathrm{V_{DC}}}^2}{\mathrm{R_{Load}P_{AC}}} \tag{3.1}$$

3.2.2 Rectifier Configurations

Rectifier designs have seen various configurations throughout the history of electronics, ranging from basic single stage envelope detector to a much complex synchronous switching rectifier. Some well-known and most used rectifier designs will be explored in this section while including their advantages, disadvantages and working concepts.

3.2.2.1 Single diode

The earliest diode invention dates back to 1874 by the German physicist Ferdinand Braun creating a 2-terminal device using a Galena crystal and thin metal wire [1], which allowed current to pass in one direction only. Though this discovery did not have any application until the year 1901 where it was used in detection of millimeter electromagnetic waves in crystal radios [2]. The single diode configuration is the most basic rectification circuit which consists of a single diode and a smoothing capacitor used for storage as presented in Figure 3.1. The output voltage of such configuration is governed by the following formula.

$$V_{out} = V_{in,max} - V_{diode} \tag{3.2}$$

V_{out}: DC output voltage

$V_{in,max}$: Amplitude of the AC signal

V_{diode}: Threshold voltage of the diode

While this circuit is simple to design and understand due to the low number of components, it doesn't offer much in terms of enhancing the output voltage that will be always be less that the amplitude of source signal due to the threshold value required to bypass the diode. The following section tackles configurations that mitigate the aforementioned limitations.

3.2.2.2 Voltage Multiplier

The earliest design of voltage multipliers was the Greinacher doubler [3] invented in 1914 by the Swiss physicist Henrich Greinacher is illustrated in Figure 3.5.

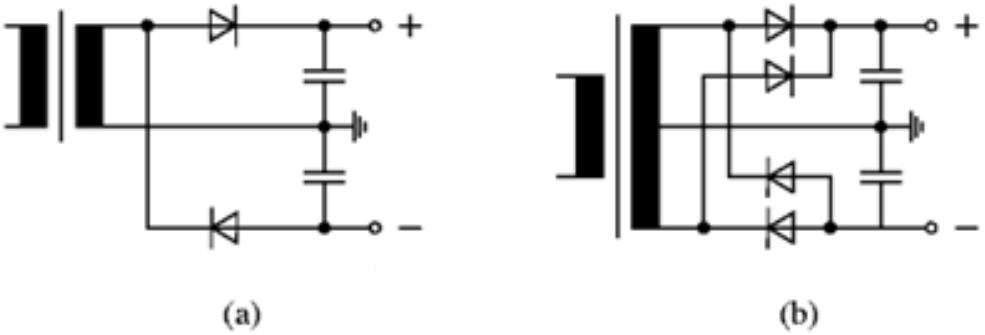

Figure 3.5 Circuit schematic of Greinacher voltage doubler [3]

The doubler uses at least 2 diode and 2 capacitors where each capacitor is charged alternatively. During the positive half of the signal, only the top diode is active leading the top capacitor to be charged to the amplitude of the signal. During the negative half, only the bottom diode is active and the capacitor is charged to the negative amplitude of the signal. Measuring the voltage across the

capacitors gives a DC voltage with a value equal to twice $V_{in,max}$. Another design worth mentioning is the Villard doubler [3] that is considered an improved design of Greinacher. Figure 3.6 depicts the design of Villard doubler.

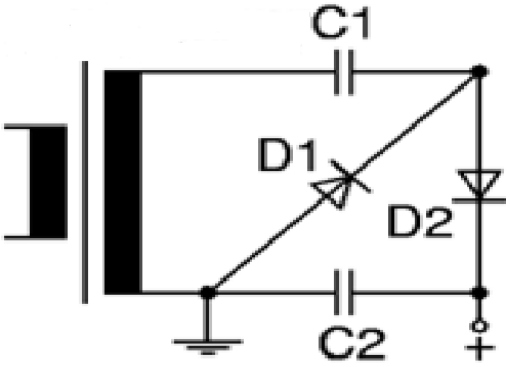

Figure 3.6 Circuit schematic of Villard voltage doubler [3]

While it relies on alternate charging of capacitors similar to the Greinacher design, all the capacitors are charged with positive DC value instead. During the negative half of the signal capacitor C1 is charged through diode D1 to $V_{in,max}$ while during the positive half capacitor C2 is charged to twice $V_{in,axm}$ due to voltage added from C1 following KVL. An advantage of such design is scalability: multiple stages of the doubler can be cascaded together to generate higher voltage values. Figure 3.7 shows a cascade of the Villard doubler.

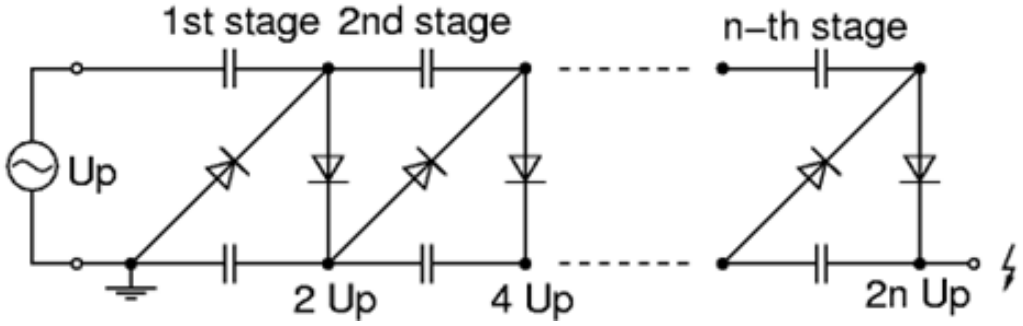

Figure 3.7 Cascaded design of Villard voltage doubler[3]

It is worth mentioning that the DC value is measured between the bottom capacitors and the ground is always a multiple of 2 while the top capacitors will have an odd multiple of the amplitude. The following equation expresses the output DC voltage of the cascaded Villard doubler.

$$V_{out} = 2N\left(V_{in,max} - V_{diode}\right) \tag{3.3}$$

$V_{in,max}$: Amplitude of AC signal

V_{diode}: Threshold voltage of the diode

N: Number of stages

3.2.3 Rectifier Choice

The rectifier configuration choice is done through the simulation results executed in the Keysight ADS (Advanced Design Systems) software. Multiple simulations have been conducted in order to choose the most efficient configuration, the number of stages of the chosen configuration and the optimal load resistance that gives the highest conversion efficiency.Harmonic Balance, S-

Parameters and Parameter Sweep simulations are used. Harmonic balance is used to obtain the steady state signal of non-linear circuits in addition to analyzing the harmonics present in the signal while S-Parameter computes the different S parameters and impedances of the circuit provided a terminal component is present in the circuit. Parameter Sweep is used to specify a variable that sweeps between values specified by Start and Stop parameters with a defined Step andexecutes the chosen simulations instances for each value of variable. In addition, Parameter Sweep can be daisy-chained in order to sweep multiple variables in conjunction with each other. Considering that this circuit is made for low power application, the input power was swept from -50dBm to -10dBm while the load resistance was swept from 50Ω to 5KΩ.The rectifier was matched to a 50Ω generator using an ideal matching network in order to avoid interference with the rectifier measurements. The configuration used was a Villard voltage doubler. Figures 3.8 and 3.9depictthe circuit schematics used for the simulations.

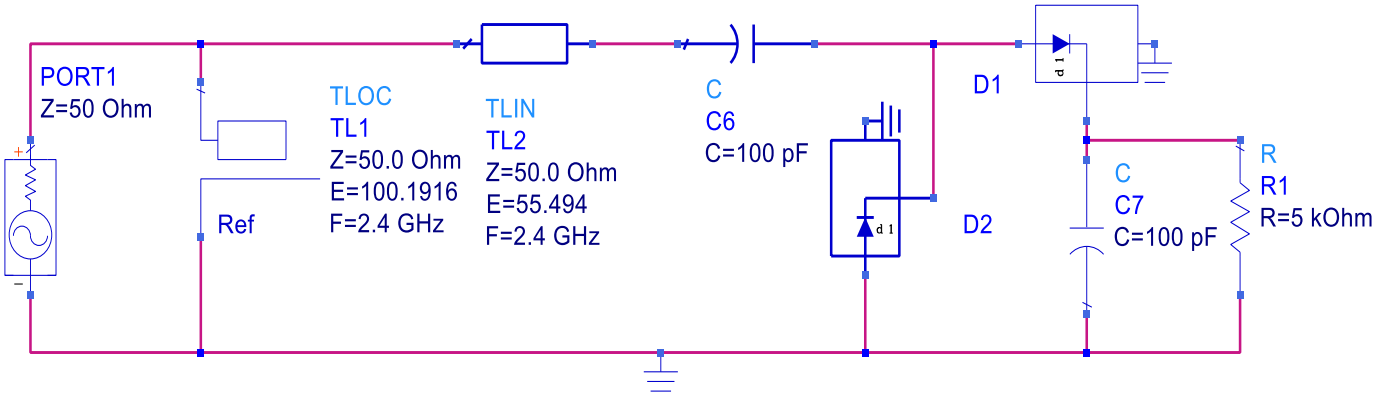

Figure 3. 8 Circuit schematic for single stage Villard doubler in ADS

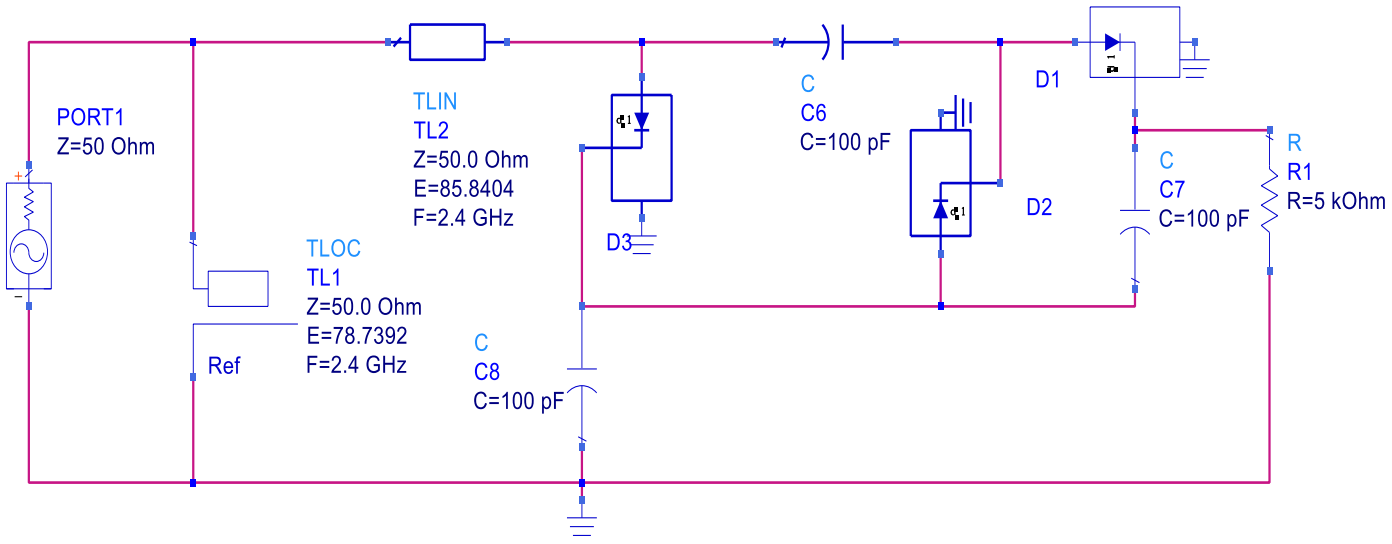

Figure 3.9 Circuit schematic for voltage multiplier in ADS

The relevant simulation results are the PCE and output DC voltage. The simulation results of circuits illustrated in Figures 3.8 and 3.9 are shown in Figures 3.10 and 3.11 respectively, where it is noticeable that the configuration of Figure 3.9 resulted in lower PCE and DC output voltage for same 5KΩ load which is explained by the presence of extra diodes in the aforementioned configuration resulting in higher losses, in addition to the low input power that struggles to surpass the threshold voltage of diodes, so increasing the number of stages results in lower overall efficiency and DC voltage rather than increasing it.

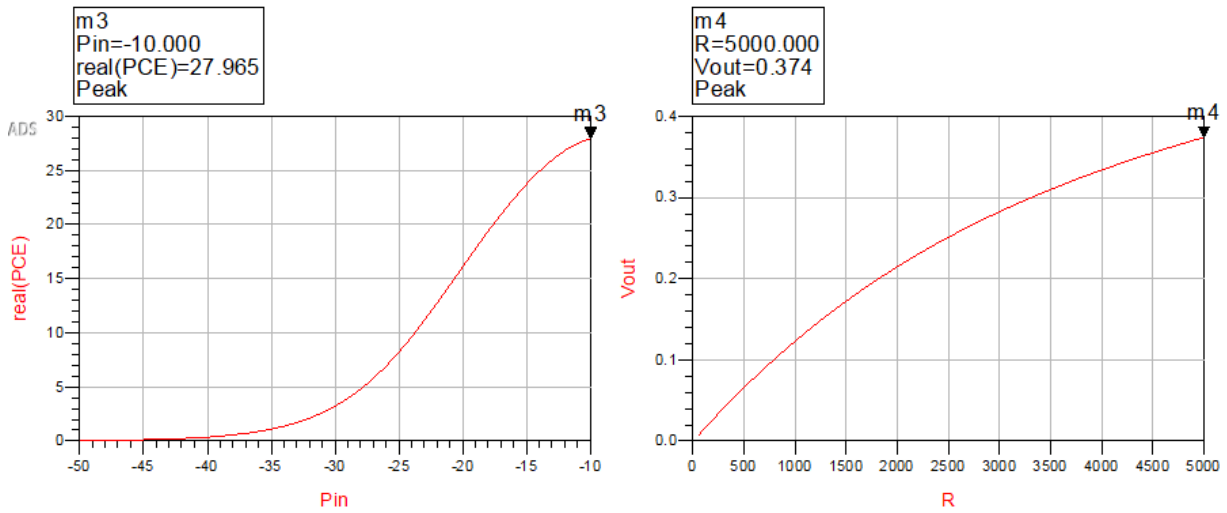

Figure 3.10 Single stage voltage doubler simulation results in ADS

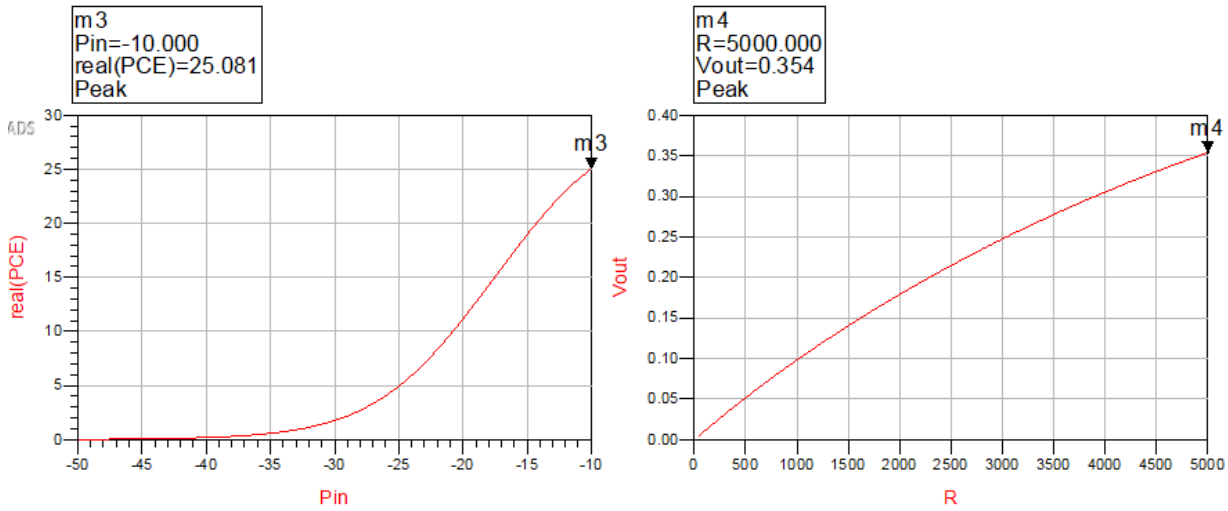

Figure 3.11 Voltage multiplier simulation results in ADS

Considering the above results, a single stage Villard doubler is chosen for the final realization using the HSMS-2850 Schottky detector diodes that has been designed and optimized for use in small signal (Pin <-20 dBm) RF applications [7]. After including physical connections using microstrip transmission lines to the rectifier circuit, the final circuit is shown in Figure 3.12.

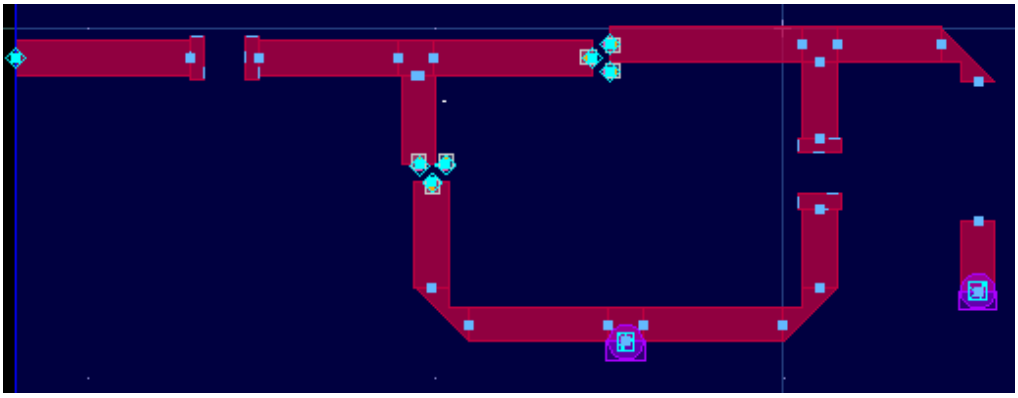

Figure 3.12 Circuit schematic for rectifier circuit

3.3 Impedance Matching Techniques

Impedance matching is a technique used to match 2 impedances and generate a desired reflection coefficient, namely used to minimize the reflections and ensure maximum power transfer. Impedance matching can realized using various networks and technologies such as lumped components or distributed elements in the form of transmission lines.

3.3.1 Lumped Elements

Lumped elements matching networks are combination of capacitors and inductors placed in different topologies such as L, T or Π matching networks and are used in low frequencies where using distributed elements is impractical due to having large dimensions (usually the length). The only drawback of such matching networks is setting the component value as accurately as possible since lumped elements usually come in standard values only and finding variable component is difficult and comes in larger dimensions compared to standard components.

3.3.1.1 L Matching Network

The simplest lumped matching network that contains only a shunt element and a series element where they are purely imaginary, so they can either be a capacitor or an inductor. The shunt element is also positioned closer to the impedance with the largest real part resulting in 8 different combinations. The general forms of L network are shown in Figures 3.13.

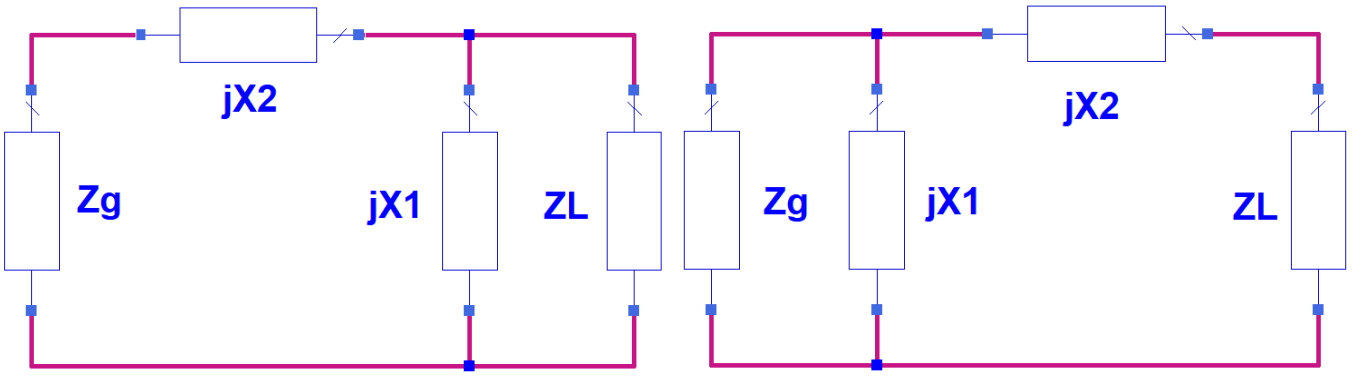

Figure 3.13 Schematic of L matching network

The synthesis equations for the above matching network are presented in Appendix II. While the L matching network is simple to design it comes at the expense of not give the designer any control over its bandwidth.

3.3.1.2 Π Matching Network

Π matching network is an extension to the L matching network while giving the designer control over the bandwidth of through the quality factor Q parameter. Higher values of Q give rise to narrower bandwidth and vice versa. Figure 3.14 illustrates the general configuration of the Π matching network.

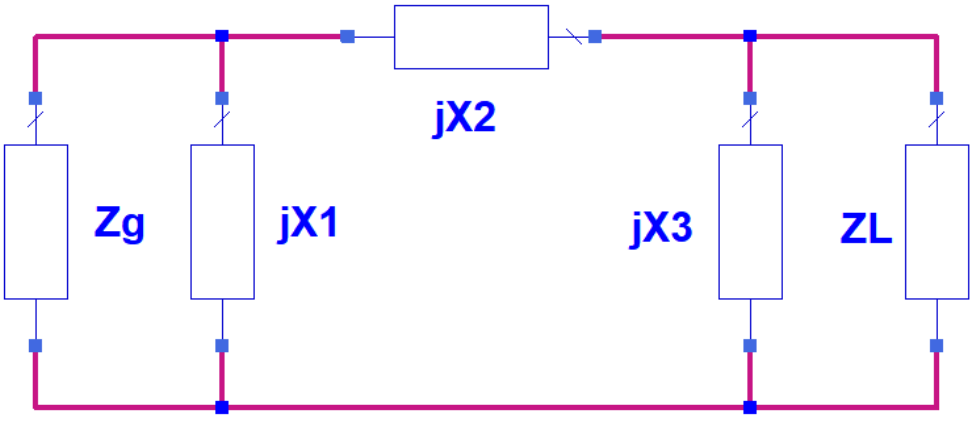

Figure 3.14 Schematic for Π matching network

3.3.2 Microstrip Technology

Microstrip was developed by ITT Federal Telecommunication Laboratories as competitor to the coaxial and waveguide technologies at the time [6]. The earliest appearance of the technology dates back to 1952 in the proceedings of the IRE (Institute of Radio Engineering) [4]. Microstrip consists of placing a thin conductor strip above a ground plane separated by a substrate of defined thickness as shown in Figure 3.15.

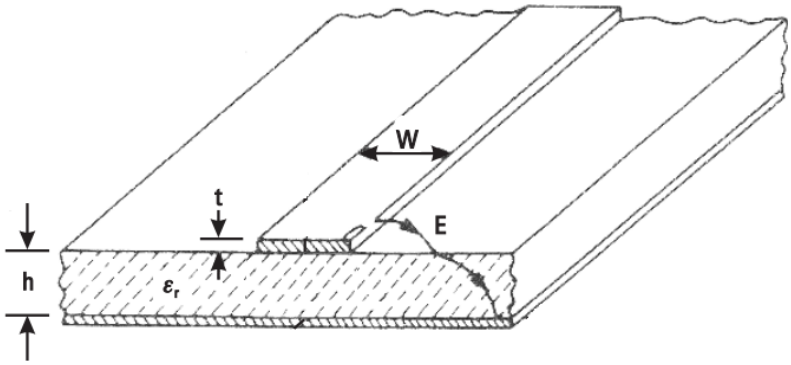

Figure 3.15 Sketch of configuration of microstrip transmission line [5]

The invention of microstrip technology revolutionized not only the RF (Radio Frequency) engineering but electronics engineering as a whole, from the invention of ICs (Integrated Circuits) to reducing the size of circuit boards and components and the creation of PCBs (Printed Circuit Board) which are indispensable for any electronics project nowadays.

3.3.3 Interdigital Elements

Due to the aforementioned limitation of the lumped elements matching network and the invention of microstrip technology, a new approach to lumped elements was devised that uses specific configuration of microstrip transmission lines to imitate the behavior of traditional lumped components over a range of frequencies while offering precise control over the value of the component in addition to having smaller dimensions in comparison. Since all the elements depend on microstrip lines as a base for their configuration, understanding the transmission line equation- that is presented below- is crucial to the design of interdigital elements.

$$Z_{in} = Z(d) = Z_0 \frac{Z_l + Z_0 \tanh(\gamma d)}{Z_0 + Z_l \tanh(\gamma d)} \tag{3.4}$$

d: Distance from load.

γ: Propagation constant of transmission line.

3.3.3.1 Capacitors

Let's consider an open-ended stub ($Z_L = \infty$) of a microstrip line with characteristic impedance Z_0, the input impedance of such a section would be equal to:

$$Z_{in} = Z_0 \frac{\infty + Z_0 \tanh(\gamma d)}{Z_0 + \infty \tanh(\gamma d)} = \frac{Z_0}{\tanh(\gamma d)} \tag{3.5}$$

Assuming small stub length ($\gamma d << 1$) results in the following input impedance.

$$Z_{in} = \frac{Z_0}{\gamma d} = \frac{G}{(wC)^2} + \frac{R}{3} + \frac{1}{jwC} \tag{3.6}$$

Figure 3.16 depict the lumped element model of an open ended microstrip stub.

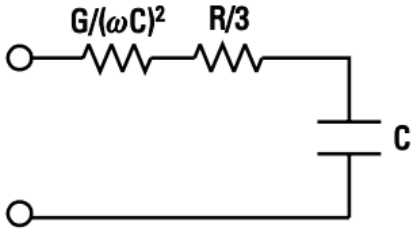

Figure 3.16 Lumped component model of a short open circuit microstrip stub [5]

Generally, the capacitance of a single stub is very small and can only be increased by increasing the length of the stub-which is already limited by the previous approximation- or reducing the characteristic impedance Z_0 by increasing the width of the stub. By analogy to actual lumped components, connecting multiple capacitors in parallel leads to an increase in the total capacitance. Figure 3.17 illustrates an interdigital capacitor and its most relevant design parameters.

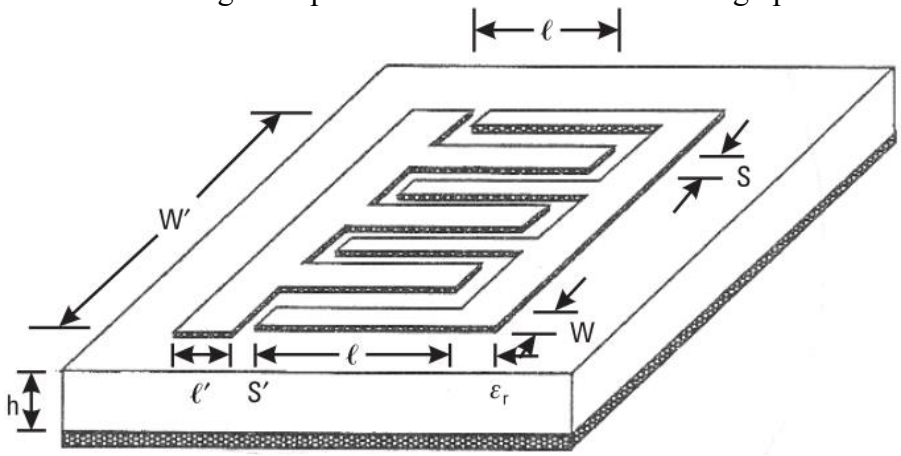

Figure 3.17 Sketch of interdigital capacitor [5]

The analysis of the above structure is not as easy as computing the individual capacitances of the stubs and summing them due to the presence of mutual inductance, skin depth, conductor and dielectric losses and dispersion effect caused by frequency of operation. Several methods have been derived in order to parameterize the capacitor as accurately as possible. Design equations for the interdigital capacitor shown in Figure 3.16 are given in Appendix III. The lumped element model of the above structure is shown in Figure 3.18.

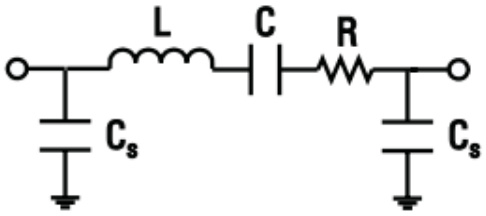

Figure 3.18 Lumped component model of interdigital capacitor [5]

The series inductance L results from the mutual inductance between the parallel stubs, the series resistance R results from the conductor material resistivity and dimensions of the stubs, the parallel capacitance C_s is generated by the separation between the stubs and the ground plane through the substrate.

3.3.3.2 Inductors

Let's consider a shorted microstrip line ($Zl = 0$) with characteristic impedance Z_0. The input impedance of the shorted line is expressed by the following equation:

$$Z_{in} = Z_0 \frac{0 + Z_0 \tanh(\gamma d)}{Z_0 + 0 \tanh(\gamma d)} = Z_0 \tanh(\gamma d) \tag{3.7}$$

Taking a short section of microstrip line ($\gamma d << 1$) results in the following approximation.

$$Z_0 \tanh(\gamma d) \approx Z_0 \gamma d = R + jwL \tag{3.8}$$

A short section of a microstrip line can be modeled using an inductor in series with a resistor. Like the previous section, the inductance generated from a short section can be insignificant and the effective method to increase it would be increasing the length of the section. Several inductor topologies have been derived in order to improve the inductance without drastically increasing the area taken by the inductor that are in analogy with their lumped counterpart as illustrated in Figure 3.19. The lumped models of the elements shown in Figure 3.19 are presented in Figure 3.20.

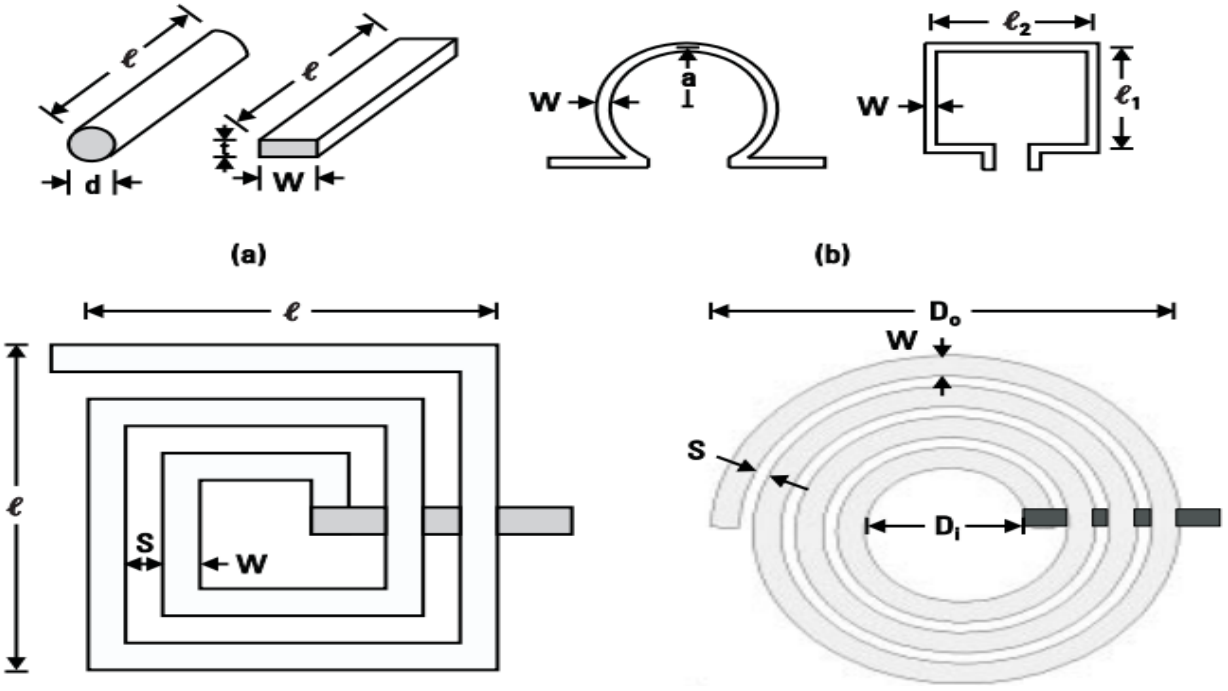

Figure 3.19 Different topologies of interdigital inductors [5]

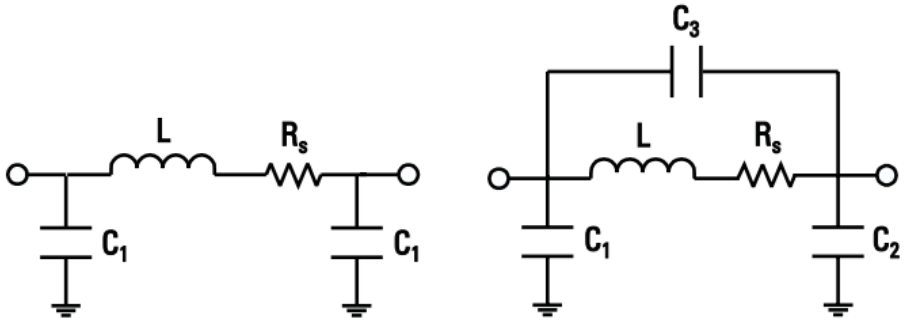

Figure 3.20 Schematic of lumped component model for section (left) and spiral (right) inductor [5]

Several methods have been derived to compute the parameters of the above structures with varying degree of accuracy as explained in [5-Chap2] and can be found in Appendix II. A more thorough

analysis of rectangular spiral inductor was done by [7] with a MATLAB code included to synthesize the inductor dimensions.

3.4 Matching Network Choice

The chosen matching network must prevent the DC signal from flowing to the RF source while also minimizing the reflection coefficient S_{11} and maximizing the forward transmission coefficient S_{21}. In this section, several lumped matching network will be simulated then the best performing circuit will be constructed using interdigital elements with the same element value then tweaked to further enhance the simulation results. Preventing DC from flowing back into the RF source limits the matching network to ones containing shunt inductor and series capacitors, so only matching networks satisfying that criteria will be considered. The simulation showed that the input impedance of the rectifier circuit was 5.01+12.653j.The matching circuits will be analyzed through PCE, DC output voltage, reflection coefficient and input impedance matching using several resistive load values ranging from 50Ω to 10KΩ.

Using an L matching network resulted in a single circuit met the specification of component choice that reached a peak efficiency of 15.459% with a 2.5 KΩ load and an output voltage of 180mV with the reflection coefficient staying below of -30 dB for most loads larger than 2KΩ. The simulation curves are displayed in Figure 3.21 through 3.24.

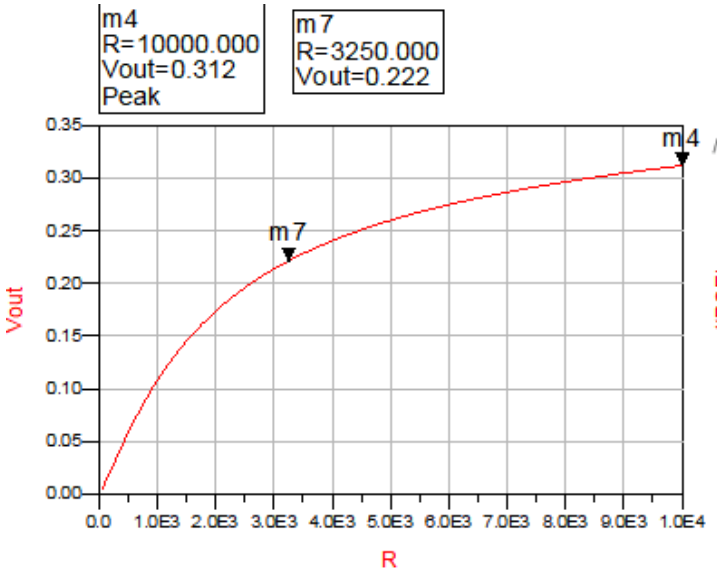

Figure 3.22 L matching network DC output voltage

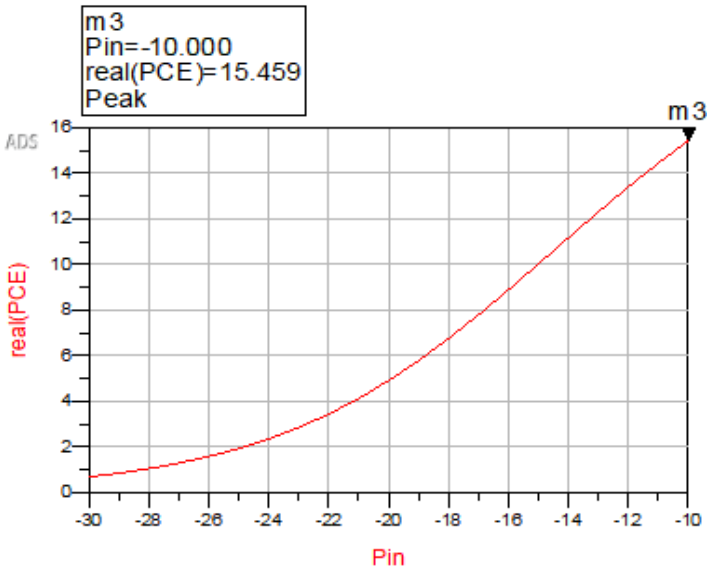

Figure 3.21 L matching network PCE

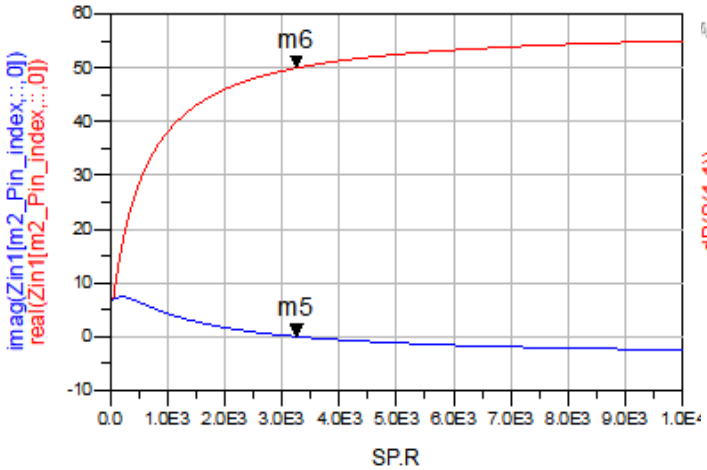

Figure 3.24 L matching network input impedance for different load resistor values

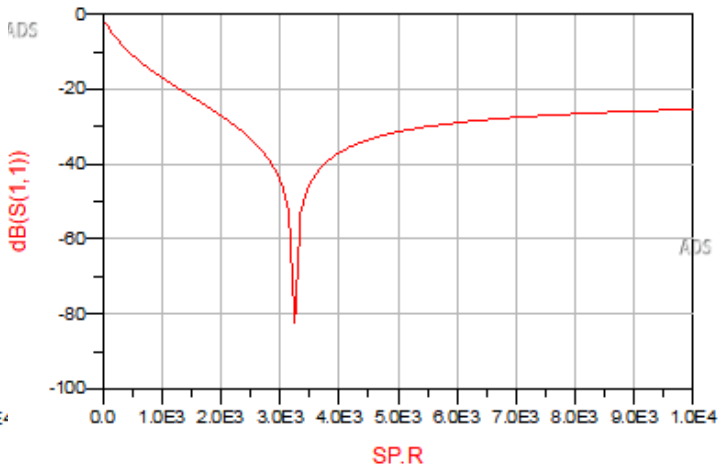

Figure 3.23 L matching network reflection coefficient

Using the Π matching network resulted in a single circuit with 2 shunt inductors and a series capacitor that has reached a peak efficiency of 15.732% with a load of 2.45KΩ and an output voltage of 200mV with a reflection coefficient below -25dB for load greater than 2KΩ. It is worth mentioning that this matching network is better at keeping the imaginary part as close to 0 as possible compared with the previous L network as illustrated in Figure. The simulation results for the first circuit are shown in Figures 3.25 to 3.28.

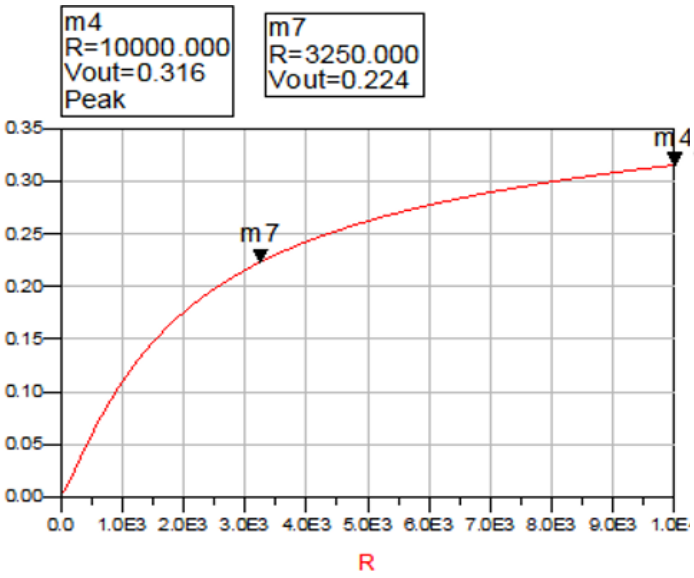

Figure3.26 Π Network DC output voltage simulation

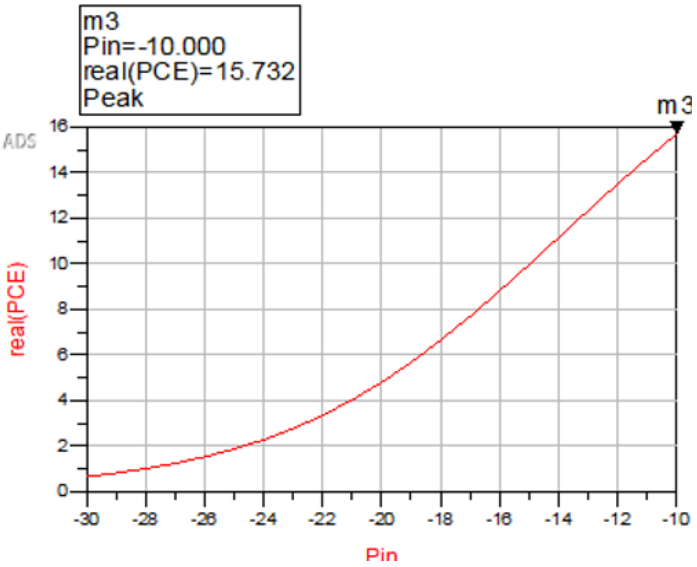

Figure 3.25 Π matching network PCE

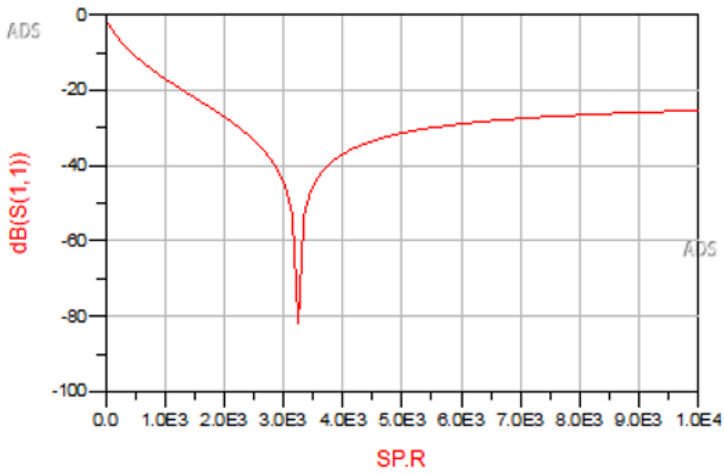

Figure 3.27 Π matching network reflection coefficient

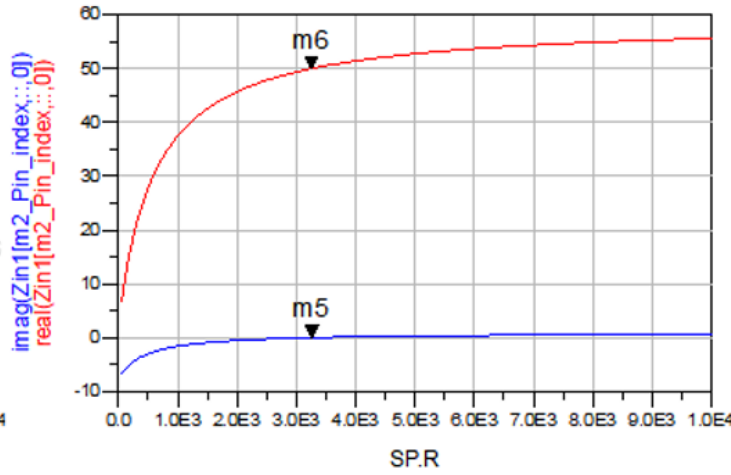

Figure 3.28 Π Network input impedance for different load resistor values

It is noticeable that the Π matching network has superior characteristics compared to the L matching network: better impedance matching, higher PCE and DC output voltage. The impedances forming the Π matching network will be created with interdigital components as previously mentioned using the equations provided in Appendix III. All the elements will be connected using actual microstrip transmission lines instead of lossless simulation links that does not affect the impedance and the ground plane is connected through metallic via holes in order to account for the losses and impedance shifting. Microstrip section inductors are used in conjunction with the capacitor depicted in Figure 3.17. The individual interdigital elements that correspond to lumped element values were created in ADS and are shown in Figure 3.29.

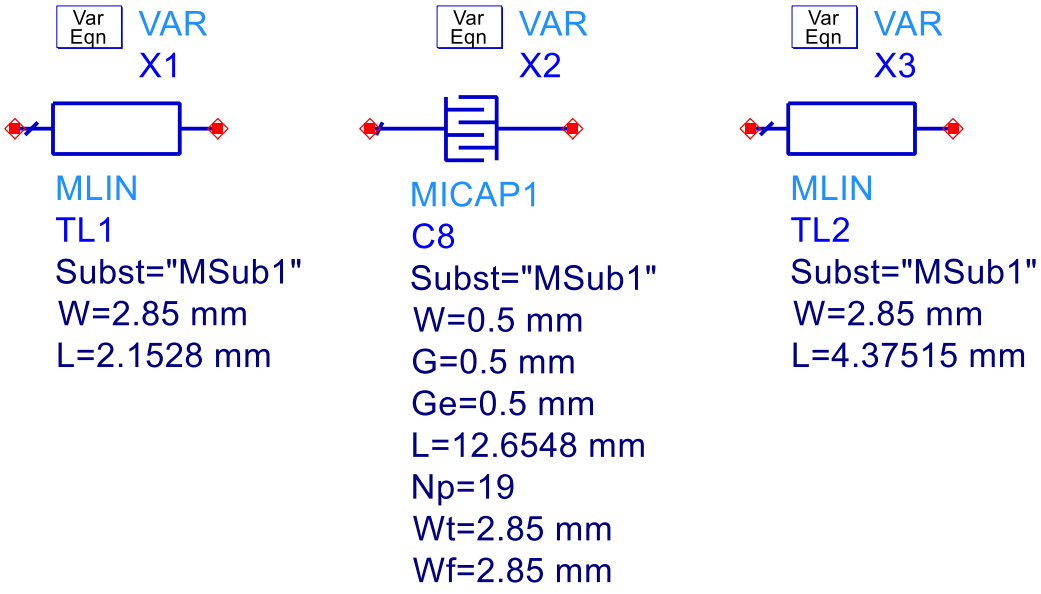

Figure 3.29 Circuit schematic of individual Interdigital that correspond to matching network elements

Including the physical connections caused a shift in the matching network which required the addition of a quarter-wave transformer and some adjustments to interdigital parameters. The circuit schematic is shown in Figure 3.30.

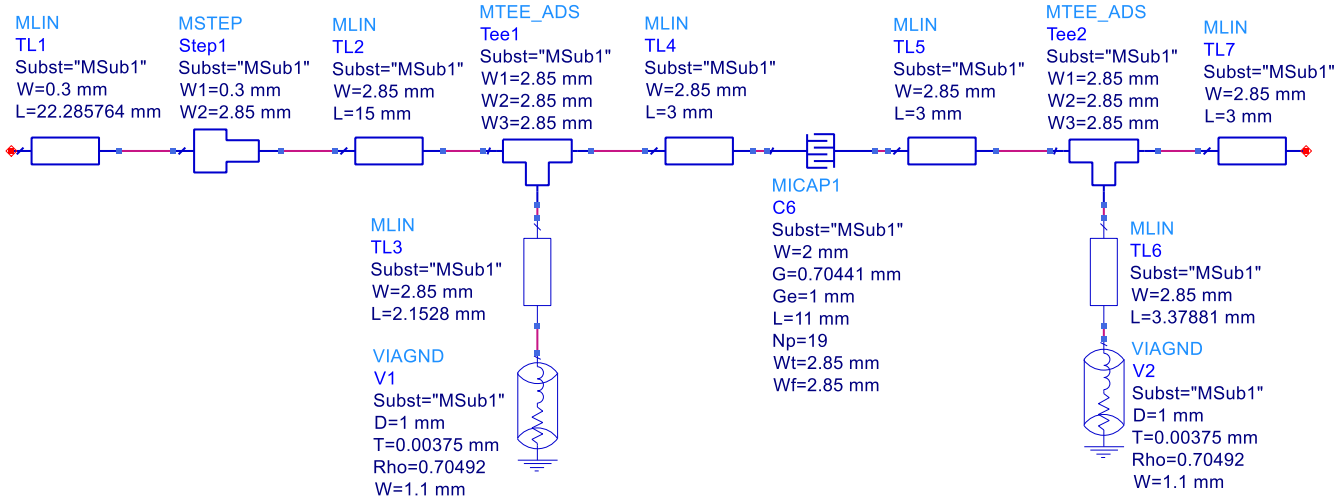

Figure 3.30 Interdigital matching network schematic

The PCB schematic of Figure 3.30 is depicted in Figure 3.31.

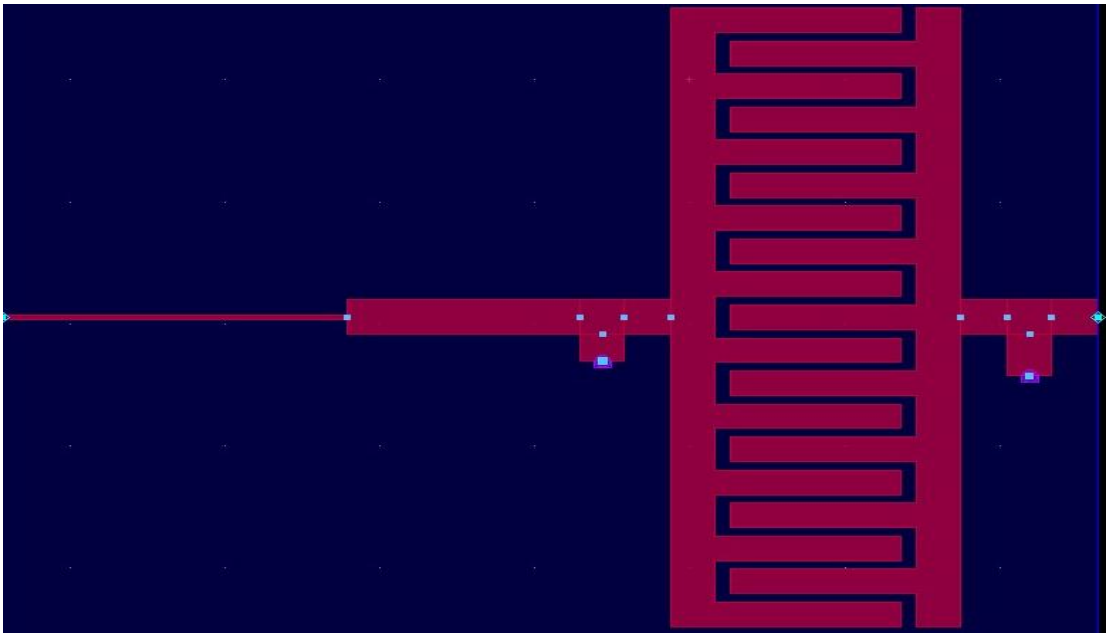

Figure 3.31 PCB schematic of interdigital matching network

The simulation results of the above schematic are shown in Figures 3.32 through 3.36.

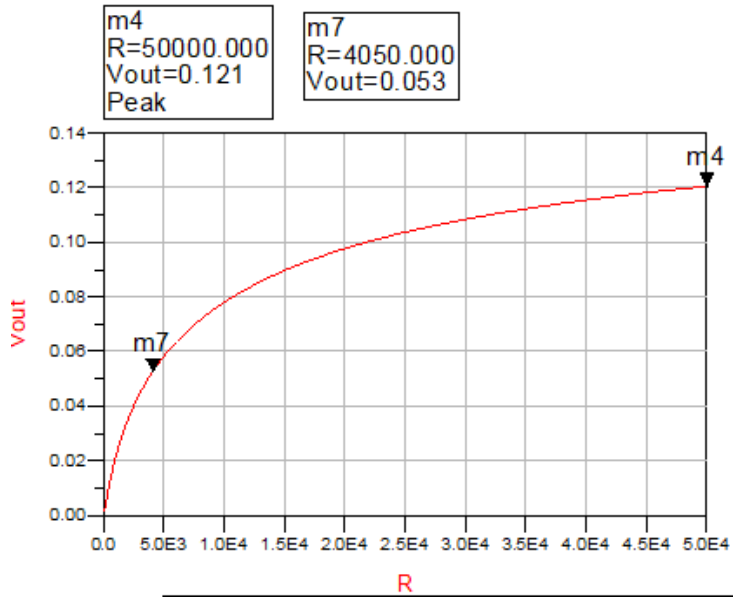

Figure 3.33 Output voltage of the circuit

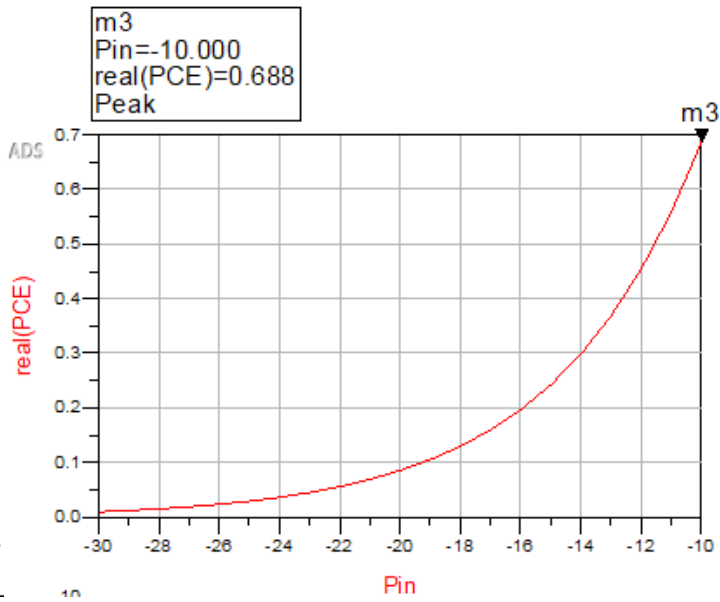

Figure 3.32 PCE of interdigital matching network

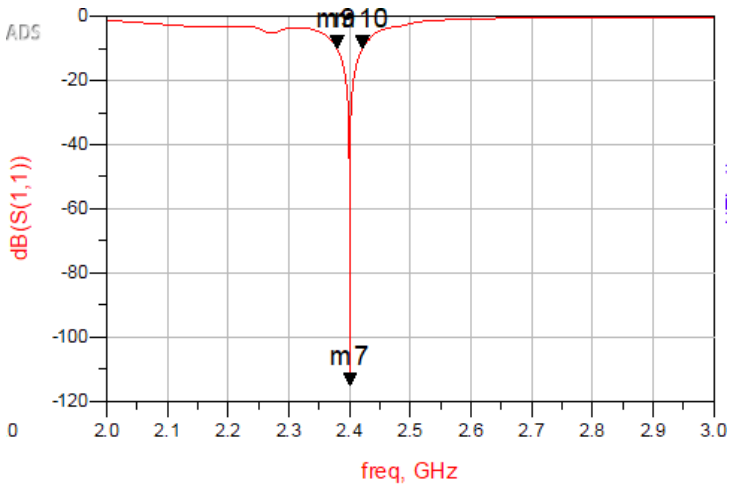

Figure 3.34 S11 of interdigital matching network

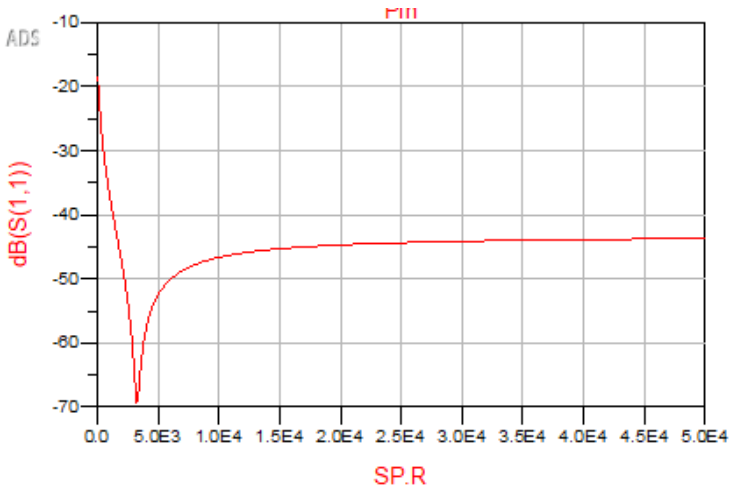

Figure 3.35 S11 of matching network using different loads

Even though the impedance was matched for all the loads in the range 5KΩ to 50KΩ as shown in Figure 3.35, the maximum PCE was 0.688% at 4KΩ load with output voltage of 53mV as illustrated in Figure 3.32 and 3.33. the results can be explained by inspecting the forward transmission coefficient S_{21} shown in Figure 3.36 which had a maximum value of -10.356dB resulting in only 31% of the input power to reach the rectifier circuit. The plot of S_{21}against frequency is shown in Figure 3.31.

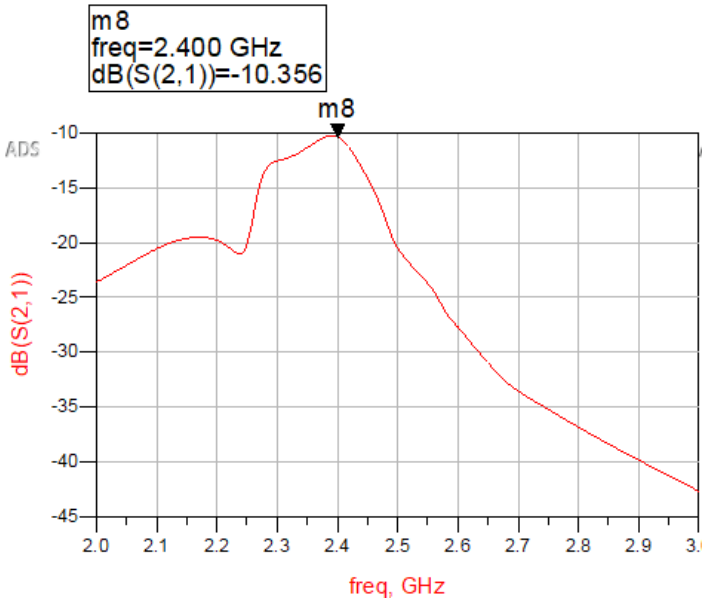

Figure 3.36 S21 of the interdigital matching network

The large number of parallel stubs in the capacitor in addition to the narrow quarter-wave transformer contributed significantly to the power losses. The losses can be mitigated by reducing the number of parallel stubs in the capacitor, removing the quarter-wave transformer and tweaking the matching network to match the impedances again. Figure 3.37 represent the schematic for the new tweaked matching network.

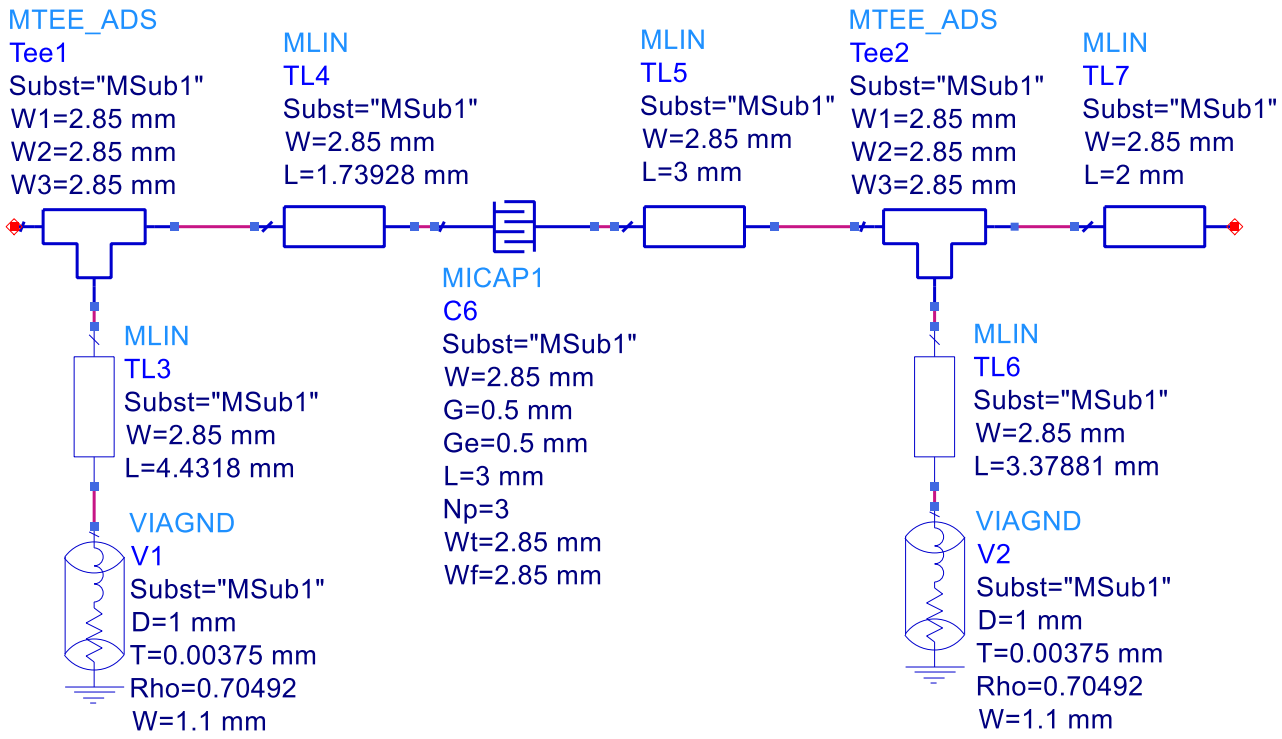

Figure 3.37 Circuit schematic of tweaked interdigital matching network

The simulation results are presented in Figures 3.38 through 3.41. The new matching network gave a peak PCE of 11.1% with an output voltage of 170mV with a load of 2.6KΩ, and all the load greater than 2KΩ resulted in a reflection coefficient lower than -30dB while also increasing the forward transmission coefficient S_{21} considerably to a value of -2.359dB.

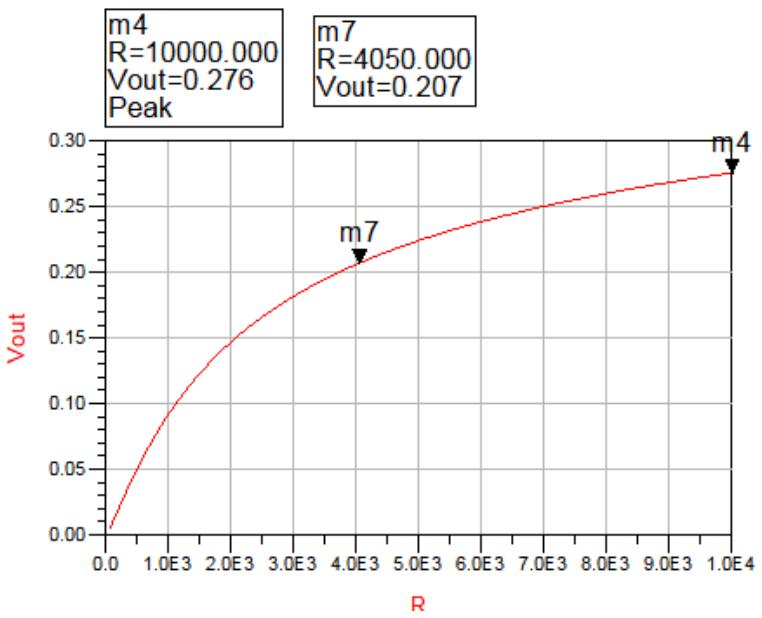

Figure 3.38 Output voltage of tweaked network

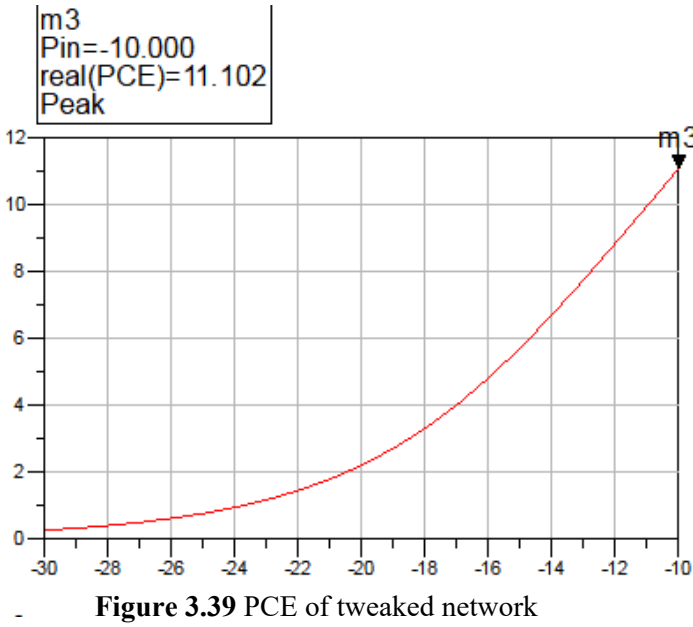

Figure 3.39 PCE of tweaked network

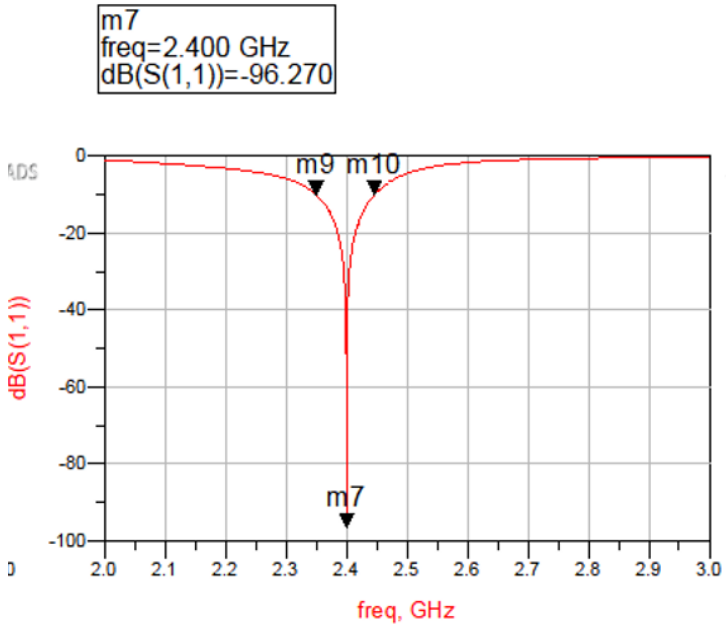

Figure 3.41 S11 of tweaked matching network

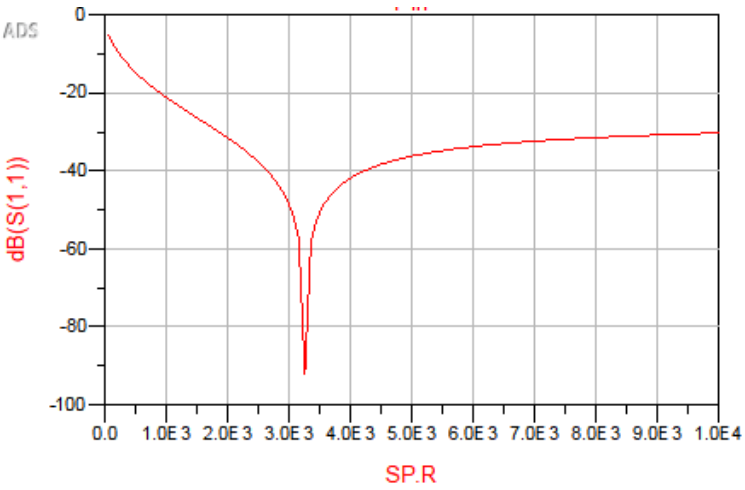

Figure 3.40 S11 of tweaked matching network with different loads

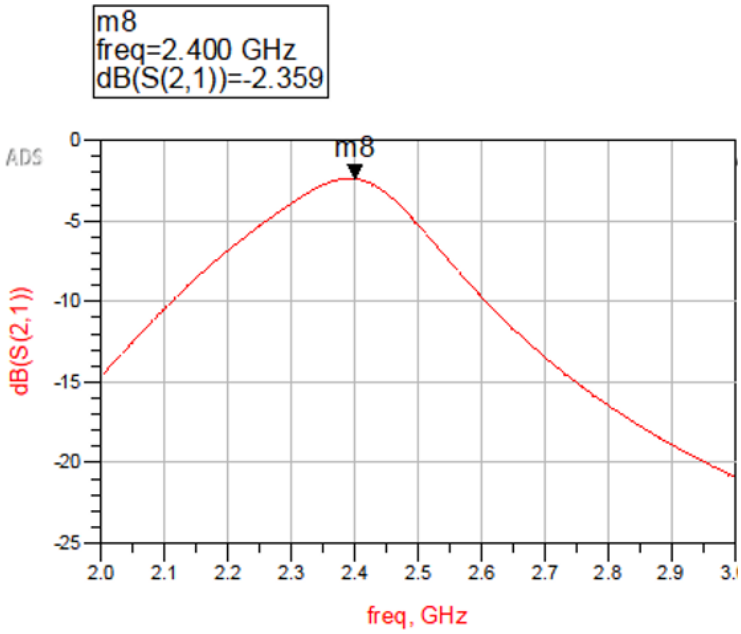

Figure 3.42 S21 of tweaked matching network

The PCB schematic of the complete circuit that was used for fabrication is shown in Figure 3.43.

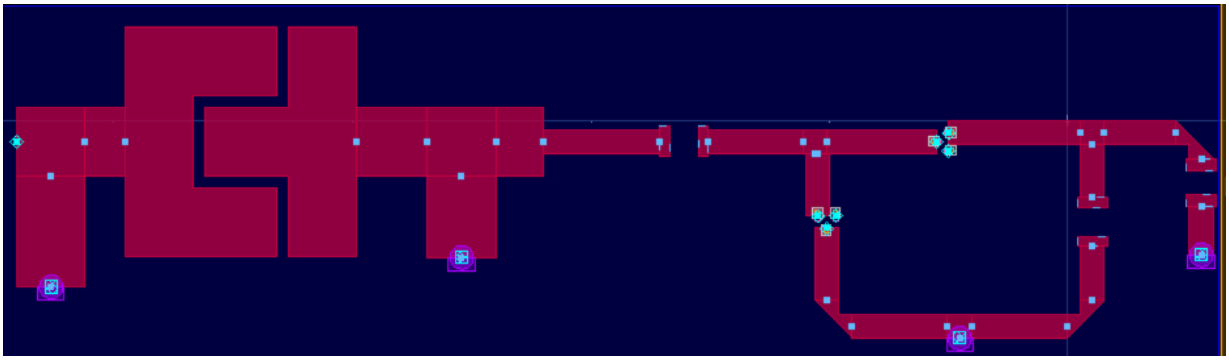

Figure 3.43 PCB schematic for the tweaked interdigital matching network and rectifier

The matching network and rectifier were not made into separate PCBs because the connector used to join the 2 circuits will affect the impedance of the rectifier and causes a mismatch and thus reducing the efficiency of the rectifier. The substrate used was an FR-4 with thickness of 1.5mm, a dielectric loss of 0.02 and the conductor used is copper strip with a thickness of 35um.

3.5 Conclusion

In conclusion, Chapter 3 provided a comprehensive overview of rectifier circuits and matching techniques relevant to rectenna design. We explored various rectifier circuit options, ultimately selecting the Villard voltage doubler for its efficiency in converting AC to DC voltage. Additionally, the chapter delved into different matching circuit types, leading to the selection of Π-matching circuit have been designed to prevent DC voltage from flowing back into the RF source. The matching network was created using interdigital lumped elements for optimal impedance matching between the antenna and rectifier in our rectenna system. These fundamental choices, backed by the theoretical background presented, establish a strong foundation for the design and subsequent fabrication of the rectenna system, which will be explored in Chapter 4.

REFERENCES

[1] Bouchouicha, D & Dupont, F &Latrach, Mohamed & Ventura, L. "Ambient RF Energy Harvesting. Renewable Energy and Power Quality Journal". (2010)

[1] https://www.computerhistory.org/siliconengine/semiconductor-point-contact-rectifier-effect-is-discovered/, visited on 20-5-2024

[2] https://www.computerhistory.org/siliconengine/semiconductor-rectifiers-patented-as-cats-whisker-detectors/, visited on 20-5-2024

[3] http://www.kronjaeger.com/hv/hv/src/mul/, visited on 21-5-2024

[4] D. D. Grieg and H. F. Engelmann, "Microstrip- A New Transmission Technique for the Klilomegacycle Range," *Proceedings of the IRE*, vol. 40, no. 12, pp. 1644-1650, Dec. 1952,

[5] Inder J. Bahl. *Lumped Elements for RF and Microwave Circuits*. Artech House. Boston London 2003.

[6] https://www.microwaves101.com/encyclopedias/history-of-microstrip, visited on 26-5-2024

[7] Agilent HSMS-285x Series Surface Mount Zero Bias Schottky Detector Diodes Data Sheet. Agilent Technologies.

Chapter 4. Results and Discussion

4.1 Introduction

After realizing the antenna and the microwave circuit consisting of rectifier and matching network that were designed in Chapter 2 and Chapter 3 respectively. This chapter focuses on validating the theoretical results in addition to comparing the experimental and simulated results. Furthermore, the RF energy harvesting system is tested.

4.2 Antenna design validation

In this section, the designed antenna has been fabricated as shown in Figure 4.1 and subjected to experimental testing. Unfortunately, that was done outside the institute due to the lack of equipment. The only information we have about the FR-4 substrate used is its thickness, h=1.5mm, no further material specific details are known for sure, therefore there may be some sort of gap between the simulated and the measured results.

Figure 4.1 Fabricated patch antenna front view (left) and back view (right)

The simulated and the measured input reflection coefficients magnitudeof the antenna in dB is shown in Figure 4.2, at first glance, the measured results confirms that our antenna resonate at 2.4GHz as the studied structure. We notice that we have a better matching and narrow bandwidth than the simulated results. These deviations are attributed to the dielectric material used in fabricating the antenna which may have a different relative permittivity than the one used in simulation. The differences are be quantified and the results are summarized in Table 4.2.

Parameters	simulated	measured	deviation
Resonant frequency	2.401GHZ	2.403GHZ	0.08%
$\lvert S_{11} \rvert$ at 2.4GHz	-31.66 dB	-36.60 dB	15.60%
Bandwidth	57.62MHz	46.35MHz	19.56%

Table 4.2 Comparison between the simulated and the measured parameters for the microstrip antenna

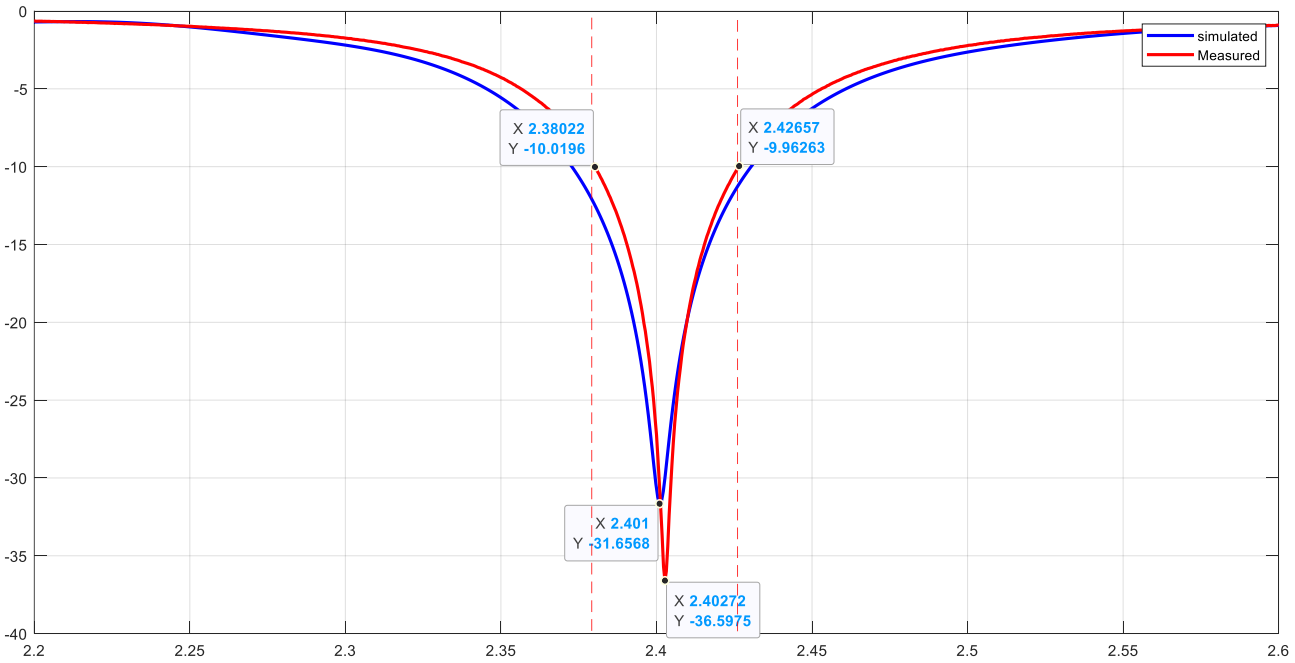

Figure 4.2 Simulated and measured magnitude of input reflection coefficient

The input impedance measured at $2.4\,GHz$ is $Z_{in} = 53.01 - j2.04\Omega$. We conclude that the fabricated antenna performs well and satisfies our project needs, since it exhibits insignificant differences compared to the simulated antenna's performance. It is important to note that there may be slight discrepancies between the values depicted in the graphs and those obtained from the laboratory equipment. This difference can be attributed to the time lag between the actual measurement and its capture for graphical representation. Additionally, experimental measurements are inherently sensitive to minor variations and susceptible to external disturbances, which can potentially influence the final results.

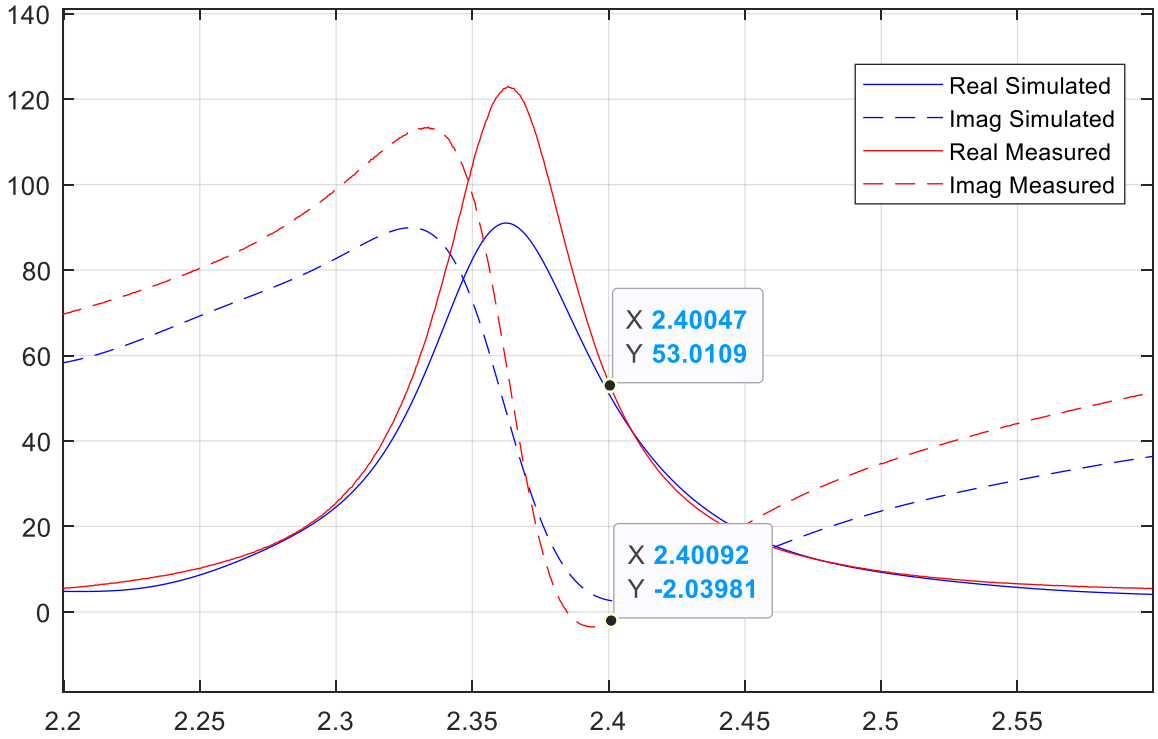

Figure 4.3 Simulated and measured input impedance.

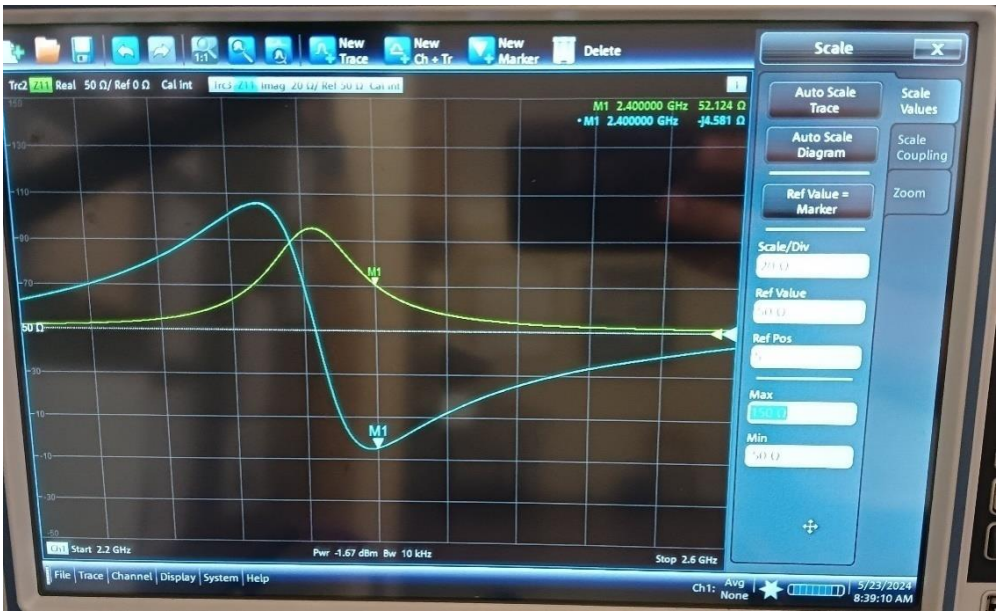

Figure 4.4 Antenna input impedance measurement using vector network analyzer

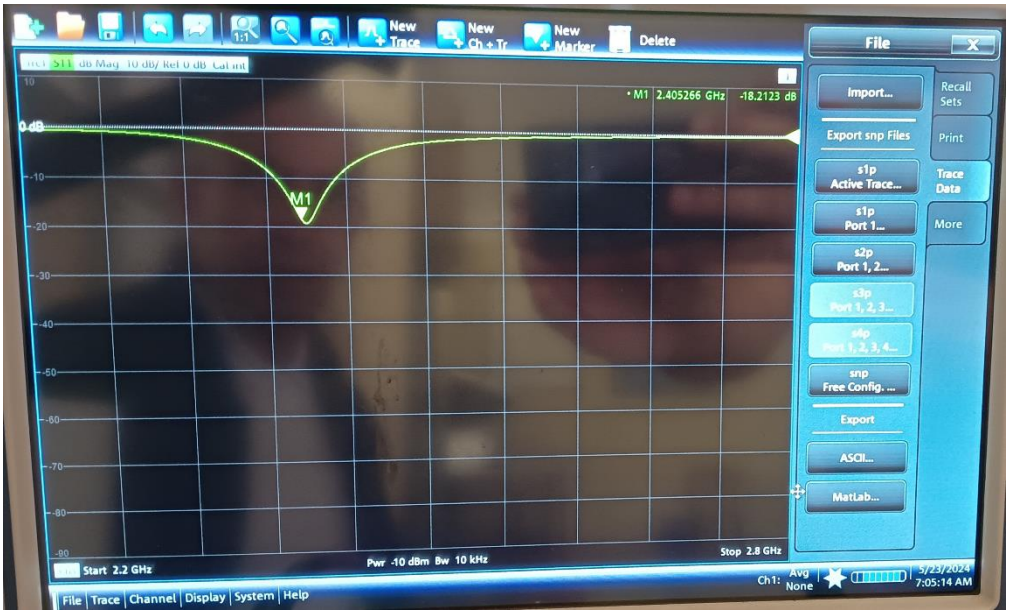

Figure 4.5 Input reflection coefficient level for the antenna using vector network analyzer

The fabricated antenna performs well and aligns closely with the results predicted by the simulations. This successful realization not only validates the design and fabrication methods but also bodes well for its performance when integrated into the rectenna system. The antenna's ability to efficiently capture RF energy, as indicated by the close match with simulations, is crucial for the overall functionality of the rectenna.

4.3 Energy Harvesting Circuit

The fabricated microwave harvesting circuit, consisting of a matching network and rectifier, is displayed in Figure 4.6. A load of 10 $k\Omega$ is employed in conjunction with 100 pF capacitors to optimize the rectenna's DC output characteristics. It's important to note that the circuit fabrication is realized at an external facility due to lack specialized equipment for fabricating microwave circuits. During the measurement phase, however, we encountered some fabrication errors that necessitated manual adjustments to the circuit using welding. This highlights the importance of close collaboration between design and fabrication stages, especially when using external facilities. Despite these challenges, the successful completion of the rectifier circuit represents a significant step towards the realization of a functional rectenna system.

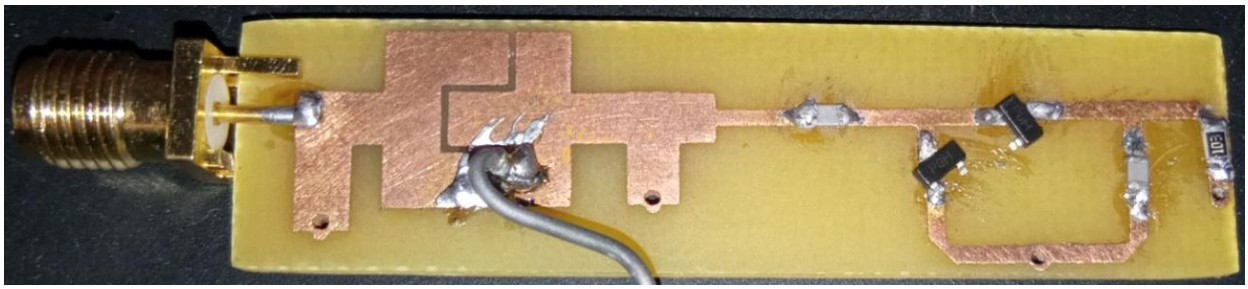

Figure 4.6 Fabricated energy harvesting circuit

The S parameters and input impedance are measured using a VNA (Vector Network Analyzer). The input impedance of the rectifier is illustrated in Figure 4.7.

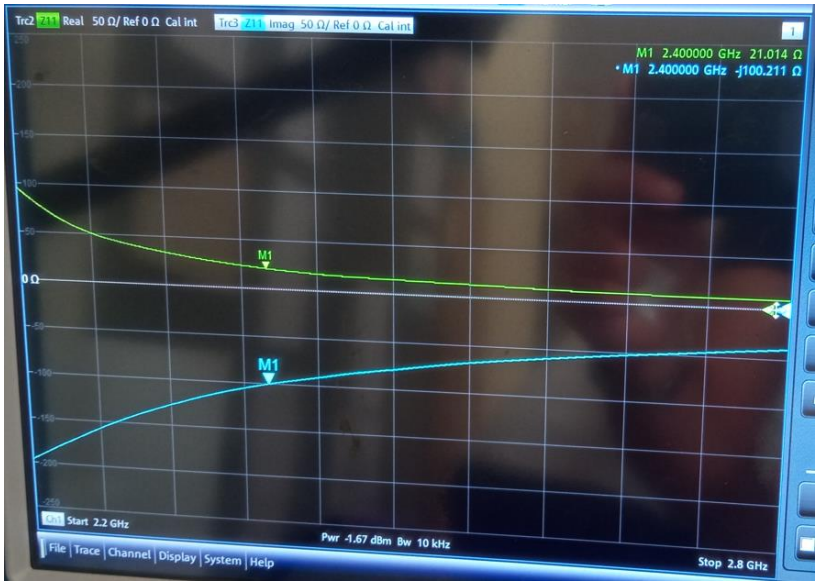

Figure 4.7 Input impedance of rectifier circuit

It is apparent that the input impedance of the rectifier is $Z_{in} = 21.014 - j100.211$ varies significantly from the simulated results where it had a value of $5.01 + 12.659j$ which can be explained by the low resolution of the PCB that is apparent in Figure 4.6 due to manufacturer lacking high quality equipment. The change in impedance will affect all subsequent measurements which is more prominent in measurement of S-parameters.

As mentioned, the mismatch of rectifier input impedance increased the reflection coefficient significantly from -30dB to -5.663dB as show in Figure 4.8, which is not acceptable to use in the energy harvesting system.

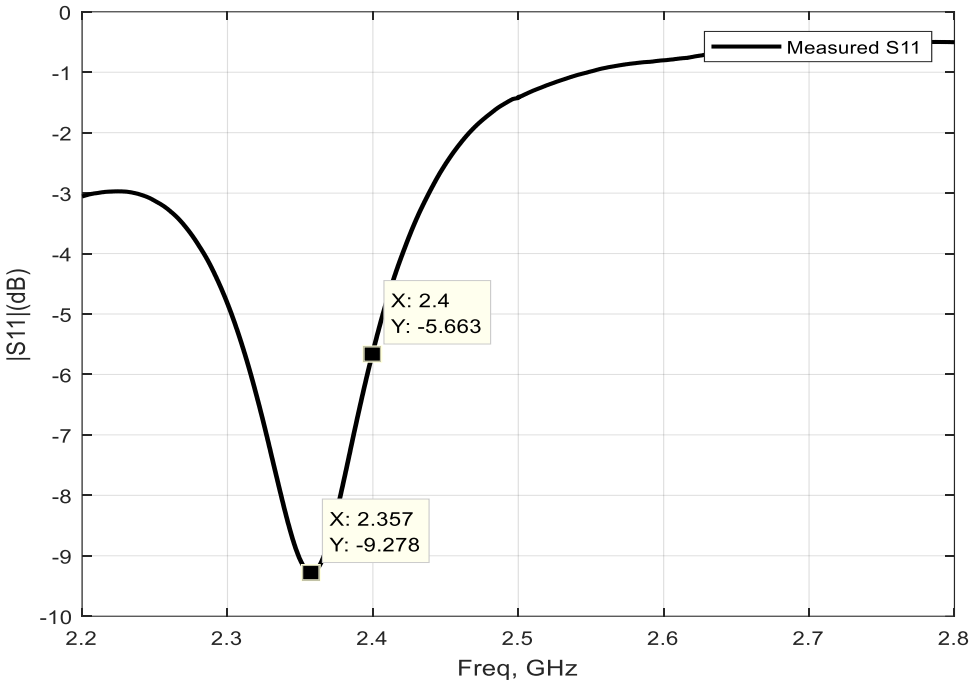

Figure 4.8 S11 of original energy harvesting circuit

In order to reduce the value of the reflection coefficient to a usable range and shift the resonant frequency manual modification was introduced on the matching network circuit. A tin welding wire is connected in different locations in the matching network while measuring the reflection coefficient and it is fixed in the position shown in Figure 4.6 which resulted in the best reflection coefficient and resonant frequency. The reflection coefficient of the modified circuit is shown in Figure 4.9.

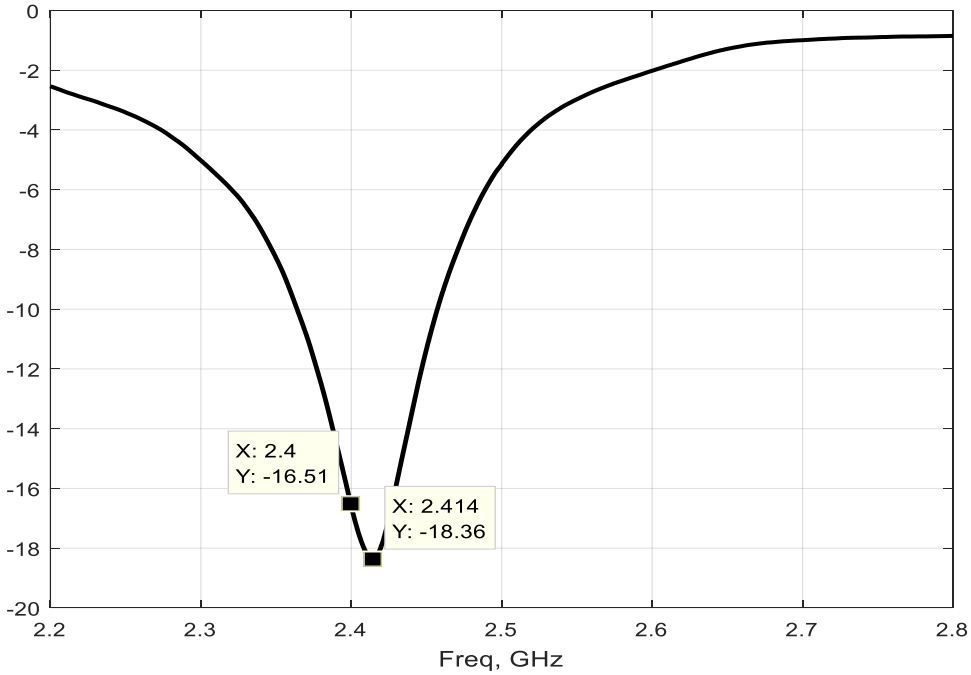

Figure 4.9 S11 of modified energy harvesting circuit

4.4 Energy Harvesting System

The measurement setup for energy harvesting system uses an RF energy generator and the same antenna of Figure 4.1 for reception and transmission that are kept as parallel to each other as possible to minimize the polarization losses and distanced by 5cm which is within the far field of the antenna. Figure 4.10 depicts the measurement setup.

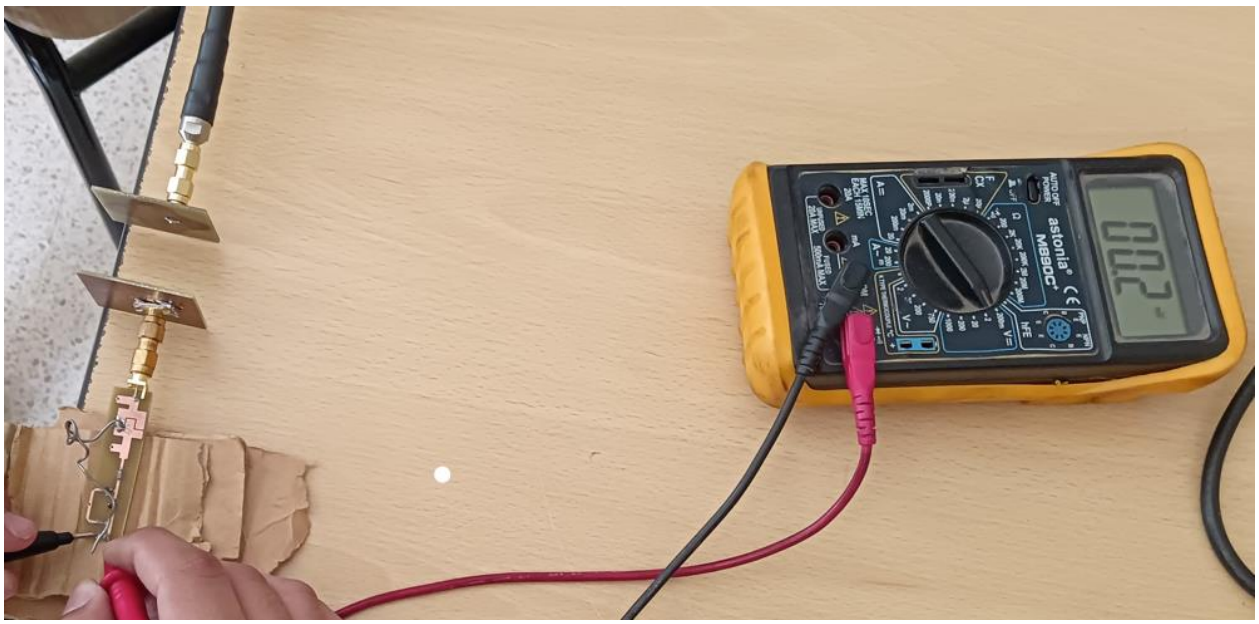

Figure 4.10 DC output voltage measurement setup

The rectenna system gives maximum output DC voltage of $5.4mV$. The DC output voltage was measured using a digital multimeter for different values of input power. The measured output voltage as a function of input power in dBm is plotted using MATLAB as shown in Figure 4.11. The power conversion efficiency of the circuit is illustrated in Figure 4.12.

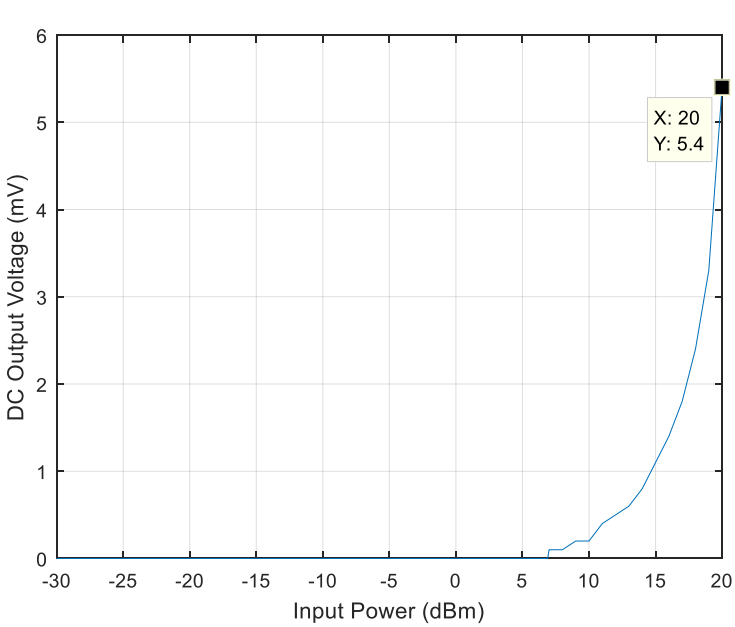

Figure 4.11 DC Output Voltage of Energy Harvesting Circuit

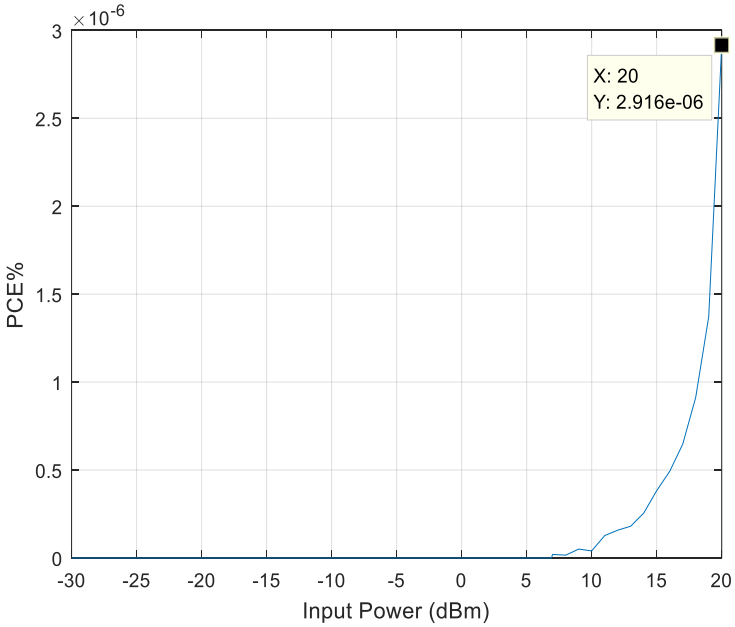

Figure 4.12 PCE of Energy Harvesting Circuit

It is noticeable that the experimental PCE, which reached a value of $2.916 \times 10^{-6}\%$, has been significantly reduced compared to the simulated results which is due to various factors, namely the radiation losses that were not accounted for in the simulation, the impedance mismatch of the rectifier circuit, the low resolution of the PCB and the use of FR4 substrate that is not recommended for RF applications.

4.5 Conclusion

Overall, this chapter demonstrates the successful development of a functional rectenna system. The fabricated antenna closely matched the simulated results, indicating an efficient design for capturing RF energy. The rectifier circuit, while requiring some adjustments during measurement, also achieved decent performance. These individual successes culminated in a functioning rectenna system with some performance reduction due to unavoidable losses. This initial achievement lays the groundwork for further optimization of the rectenna design to minimize losses and maximize its RF energy harvesting efficiency.

GENERAL CONCLUSION

The aim of this project is to make a contribution to the Electromagnetic Power Harvesting field which represents a significant advancement in the renewable energy sources technologies. Through this research, several key contributions to the design and optimization of this system have been made. At first, background in theory rectenna has been gathered alongside the different approaches and similar work in this field.

The patch antenna is designed to resemble a clover leaf in shape operating at 2.4 GHz achieved using a parametric study on the patch dimension and feed point. The microstrip antenna impedance is set using coaxial feeding technique for efficient power delivery. Simulations resulted in narrow bandwidth with minimum reflections and matched to 50Ω transmission line.

The Villard Voltage Doubler rectifier configuration is selected throughout many simulations executed in Keysight ADS. To prevent interference with the rectifier measurements, an ideal matching network has been used to match a 50Ω generator. At the end, a Π-matching network has been selected under some specific guidelines to prevent DC signal from flowing to the RF source, as well as for minimum reflection coefficient and maximum transfer of forward voltage gain. The matching network is designed using interdigital lumped elements which have never been used for energy harvesting applications.

Our work is backed with practical measurements for each part of the rectenna to validate our simulation and theoretical work. Considering the manufacturing limitations, the lack of components and material and the absence of high-resolution measuring devices, we achieved acceptable results.

As a further work, we may suggest improvements in the following:

- Array antenna instead of only one patch can significantly increase the Gain of the antenna.
- Using Wilkinson power combiner to merge the energy from multiple antennas.
- Implement the design on a real low-power consumption device.
- Use the rectenna for wireless power transfer system to power a specific device not collecting the ambient EM waves.
- Include DC boosting circuit for to enhance the DC output voltage.
- Use materials for substrate and conductor that are suitable for RF applications.
- Fabricate a higher resolution PCB that is more accurate to the Design schematic.

APPENDIX I
MICROWAVE TRANSMISSION LINE PARAMETERS

This appendix is reserved to the equations used to calculate the microstrip transmission line parameters taken from [h pp430-433]. In the following equations all the dimensions are in Micron and frequency is in GHz. The parameters are presented in Figure 3.14.

The characteristic impedance is calculated as follows:

$$Z_0 = \begin{cases} \dfrac{\eta}{2\pi\sqrt{\varepsilon_{re}}}\ln\left(\dfrac{8h}{W_e}+0.25\dfrac{W_e}{h}\right), & \dfrac{W_e}{h}<0 \\ \dfrac{\eta}{\sqrt{\varepsilon_{re}}}\left\{\dfrac{W_e}{h}+1.393+0.67\ln\left(\dfrac{W_e}{h}+1.444\right)\right\}^{-1}, & \dfrac{W_e}{h}\geq 0 \end{cases} \quad \text{(I. 1)}$$

$$\frac{W_e}{h} = \begin{cases} \dfrac{W}{h}+\dfrac{1.25}{\pi}\dfrac{t}{h}\left\{1+\ln\left(\dfrac{4\pi W}{t}\right)\right\}, & \dfrac{W}{h}<0.5\pi \\ \dfrac{W}{h}+\dfrac{1.25}{\pi}\dfrac{t}{h}\left\{1+\ln\left(\dfrac{2h}{t}\right)\right\}, & \dfrac{W}{h}\geq 0.5\pi \end{cases} \quad \text{(I. 2)}$$

$$\eta = 120\pi$$

The effective relative permittivity:

$$\varepsilon_{re} = \frac{\varepsilon_r+1}{2}+\frac{\varepsilon_r-1}{2}F\left(\frac{W}{h}\right)-C \quad \text{(I. 3)}$$

$$F\left(\frac{W}{h}\right) = \begin{cases} \left(1+\dfrac{12h}{W}\right)^{-\frac{1}{2}}+0.041\left(1-\dfrac{W}{h}\right)^2 & ,\dfrac{W}{h}<1 \\ \left(1+\dfrac{12h}{W}\right)^{-\frac{1}{2}} & ,\dfrac{W}{h}\geq 1 \end{cases} \quad \text{(I. 4)}$$

$$C = \frac{\varepsilon_r-1}{4.6}\frac{t}{\sqrt{Wh}} \quad \text{(I. 5)}$$

Taking into account the effect of dispersion caused by the frequency on the microstrip parameters, the following formulas are used:

$$Z_0(f) = Z_0\frac{\varepsilon_{re}(f)-1}{\varepsilon_{re}-1}\sqrt{\frac{\varepsilon_{re}}{\varepsilon_{re}(f)}} \quad \text{(I. 6)}$$

$$\varepsilon_{re}(f) = \varepsilon_r-\frac{\varepsilon_r-\varepsilon_{re}}{1+\left(\frac{f}{f_{50}}\right)^m} \quad \text{(I. 7)}$$

$$f_{50} = \frac{f_{k,TM0}}{0.75+\frac{\left\{0.75-\frac{0.332}{\varepsilon_r{}^{1.73}}\right\}W}{h}} \quad \text{(I. 8)}$$

$$f_{k,TM0} = \frac{c\tan^{-1}\left(\varepsilon_r\sqrt{\frac{\varepsilon_{re}-1}{\varepsilon_r-\varepsilon_{re}}}\right)}{2\pi h\sqrt{\varepsilon_r-\varepsilon_{re}}} \quad \text{(I. 9)}$$

$$m = m_0 m_c \quad \text{(I. 10)}$$

$$m_0 = 1 + \frac{1}{1 + \sqrt{\frac{W}{h}}} + 0.32 \left(\frac{1}{1 + \sqrt{\frac{W}{h}}} \right)^3 \qquad \text{(I. 11)}$$

$$m_c = \begin{cases} 1 + \frac{1.4}{1 + \frac{W}{h}} \left\{ 0.15 - 0.235 e^{-\frac{0.45f}{f_{50}}} \right\}, & \frac{W}{h} < 0 \\ 1 \qquad\qquad\qquad\qquad\qquad , & \frac{W}{h} \geq 0 \end{cases} \qquad \text{(I. 12)}$$

APPENDIX II
LUMPED COMPONENT MATCHING NETWORKS

The appendix is reserved for synthesis formulas of lumped component matching networks focusing only on L and Π configurations.

L matching network can have 2 different configurations as illustrated in Figure 3.12. The shunt element will always be closer to the impedance with the largest real part. Let Z_A be the impedance with the largest real part and R_A and X_A be its real and imaginary parts respectively. Let Z_C be the other impedance and let R_C and X_C be its real and imaginary parts respectively. The following equations are used to calculate the impedance values X_1 and X_2.

$$X_1 = \frac{X_A \pm R_A Q}{\frac{R_A}{R_C} - 1} \tag{II. 1}$$

$$X_2 = -(X_C \pm R_C Q) \tag{II. 2}$$

$$Q = \sqrt{\frac{R_A}{R_C} - 1 + \frac{{X_A}^2}{R_A R_C}} \tag{II. 3}$$

The Π matching network can be analyzed by dissecting it into 2 L matching network that are matched to a hypothetical resistance R_H with a value smaller than the real part of load or generator impedances. After choosing the value of Q, the following equations are used to compute the impedances values X1, X2 and X3 shown in Figure II.1.

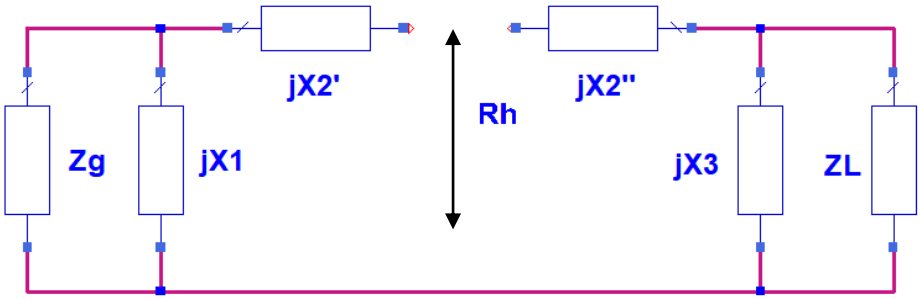

Figure II.1 Schematic of dissected Π matching network

$$if\ R_L < R_g: \begin{cases} Q_1 = Q \\ R_h = \dfrac{{R_g}^2 + {X_g}^2}{R_g\left({Q_1}^2 + 1\right)} \\ Q_2 = \sqrt{\dfrac{R_L}{R_g} - 1 + \dfrac{{X_L}^2}{R_h R_L}} \end{cases} \tag{II. 4}$$

$$if\ R_L > R_g: \begin{cases} Q_2 = Q \\ R_h = \dfrac{{R_L}^2 + {X_L}^2}{R_L\left({Q_2}^2 + 1\right)} \\ Q_2 = \sqrt{\dfrac{R_g}{R_h} - 1 + \dfrac{{X_g}^2}{R_h R_g}} \end{cases} \quad \text{(II. 5)}$$

$$X_1 = \frac{X_g \pm R_g Q_1}{\frac{R_g}{R_h} - 1} \quad \text{(II. 6)}$$

$$X_3 = \frac{X_L \pm R_L Q_2}{\frac{R_L}{R_h} - 1} \quad \text{(II. 7)}$$

$${X_2}' = \mp R_h Q_1 \quad \text{(II. 8)}$$

$${X_2}'' = \mp R_h Q_2 \quad \text{(II. 9)}$$

$$X_2 = {X_2}' + {X_2}'' \quad \text{(II. 10)}$$

APPENDIX III
INTERDIGITAL COMPONENTS FORMULAS

This appendix is dedicated to the calculation of interdigital lumped components values.

Capacitorused for these calculations is the one illustrated in Figure 3.16.

$$C = (\varepsilon_r + 1)\ell[(N-3)A_1 + A_2](pF) \quad \text{(III. 1)}$$

$$A_1 = 4.409\tanh[0.55(\frac{h}{W})^{0.45}] * 10^{-6}\left(\frac{pF}{um}\right) \quad \text{(III. 2)}$$

$$A_2 = 9.92\tanh[0.52(\frac{h}{W})^{0.5}] * 10^{-6}\left(\frac{pF}{um}\right) \quad \text{(III. 3)}$$

$$R = \frac{4}{3}\frac{\ell}{NW}R_s \quad \text{(III. 4)}$$

$$L = \frac{Z_0\sqrt{\varepsilon_{re}}}{c}\ell \quad \text{(III. 5)}$$

$$f_{res} = \frac{1}{2\pi\sqrt{LC}} \quad \text{(III. 6)}$$

$$C_e = \frac{C}{1 - \left(\frac{f}{f_{res}}\right)^2} \quad \text{(III. 7)}$$

C: total capacitance

ℓ: Length of the stub.

L: parasitic inductance

R_s: sheet resistance of the conductor (ohm/square)

f_{res}: resonant frequency

C_e: effective capacitance.

f: operating frequency.

For the inductor the following formulas are used. The section and spiral inductor areshownin figure 3.3 and 3.4 respectively.

Section or loop:

$$L(nH) = \begin{cases} 2 * 10^{-4}\ell\left[\ln\left(\frac{\ell}{W+t}\right) + 1.193 + \frac{W+t}{3\ell}\right]K_g & section \\ 1.257 * 10^{-3}a\left[\ln\left(\frac{a}{W+t}\right) + 0.078\right]K_g & loop \end{cases} \quad \text{(III. 8)}$$

$$R_s = \frac{KR_{sh}\ell}{2(W+t)}(\Omega) \quad \text{(III. 9)}$$

$$C_1 = 16.67 * \frac{10^{-4}l\sqrt{\varepsilon_{re}}}{Z_0}(pF) \quad \text{(III. 10)}$$

Spiral:

$$L = 0.03937\frac{a^2n^2}{8a+11c}K_g(nH) \tag{III. 11}$$

$$a = \frac{D_0 + D_i}{4}, \quad c = \frac{D_0 - D_i}{2} \tag{III. 12}$$

$$R_s = \frac{KR_{sh}\pi an}{W}(\Omega) \tag{III. 13}$$

$$C_3 = 3.5 * 10^{-5}D_0 + 0.06 \quad (pF) \tag{III. 14}$$

$$K_g = 0.57 - 0.145 * \frac{W}{h}, \quad \frac{W}{h} > 0.05 \tag{III. 15}$$

$$K\begin{cases} 1.4 + 0.217\ln\left(\frac{W}{5t}\right) & Section\ and\ loop \\ 1 + 0.333\left(1 + \frac{S}{W}\right) & Spiral \end{cases} \tag{III. 16}$$

APPENDIX IV
HSMS-2850 SCHOTTKY DIODE ELECTRIC SPECIFICATIONS

This appendix is reserved for the most important electric specifications related to the Schottky diode HSMS-2850 taken from its datasheet [7].

Tableau VI.1 HSMS-2850 DC electrical specification

Part Number HSMS-	Package Marking Code[1]	Lead Code	Configuration	Maximum Forward Voltage V_F (mV)		Maximum Reverse Leakage, IR (μA)	Typical Capacitance C_T (pF)
285B 285C 285L 285P	P0 P2 PL PP	B C L P	Single[2] Series Pair[2,3] Unconnected Trio Bridge Quad	150	250	175	0.30
Test Conditions				I_F = 0.1 mA	I_F = 1.0 mA	VR=2V	V_R = 0.5 V to –1.0V f = 1 MHz

Tableau VI.2 HSMS-2850 RF electrical specifications

Part Number HSMS-	Typical Tangential Sensitivity TSS (dBm) @ f = 915 MHz	Typical Voltage Sensitivity γ (mV/μW) @ f = 915 MHz	Typical Video Resistance RV (KΩ)
2850 2852 2855 285B 285C 285L 285P	–57	40	8.0
Test Conditions	Video Bandwidth = 2 MHz Zero Bias	Power in = –40 dBm R_L = 100 KΩ, Zero Bias	Zero Bias

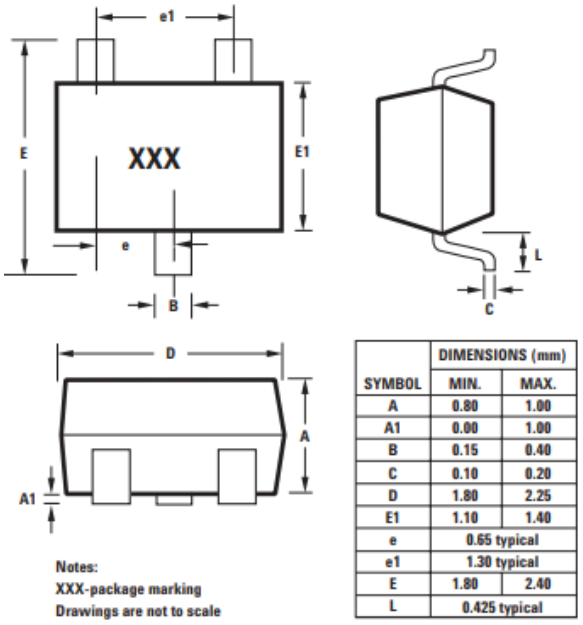

SYMBOL	DIMENSIONS (mm) MIN.	MAX.
A	0.80	1.00
A1	0.00	1.00
B	0.15	0.40
C	0.10	0.20
D	1.80	2.25
E1	1.10	1.40
e	0.65 typical	
e1	1.30 typical	
E	1.80	2.40
L	0.425 typical	

Figure VI.1 HSMS-2850 Schottky dimensions [7]